

Influence maximization in complex networks through optimal percolation

Flaviano Morone and Hernán A. Makse

Levich Institute and Physics Department,

City College of New York, New York, NY 10031

Abstract

The whole frame of interconnections in complex networks hinges on a specific set of structural nodes, much smaller than the total size, which, if activated, would cause the spread of information to the whole network [1]; or, if immunized, would prevent the diffusion of a large scale epidemic [2, 3]. Localizing this optimal, i.e. minimal, set of structural nodes, called influencers, is one of the most important problems in network science [4, 5]. Despite the vast use of heuristic strategies to identify influential spreaders [6–14], the problem remains unsolved. Here, we map the problem onto optimal percolation in random networks to identify the minimal set of influencers, which arise by minimizing the energy of a many-body system, where the form of the interactions is fixed by the non-backtracking matrix [15] of the network. Big data analyses reveal that the set of optimal influencers is much smaller than the one predicted by previous heuristic centralities. Remarkably, a large number of previously neglected weakly-connected nodes emerges among the optimal influencers. These are topologically tagged as low-degree nodes surrounded by hierarchical coronas of hubs, and are uncovered only through the optimal collective interplay of all the influencers in the network. Eventually, the present theoretical framework may hold a larger degree of universality, being applicable to other hard optimization problems exhibiting a continuous transition from a known phase [16].

The optimal influence problem was initially introduced in the context of viral marketing [1], and its solution was shown to be NP-hard [4] for a generic class of linear threshold models of information spreading [17, 18]. Indeed, finding the optimal set of influencers is a many-body problem in which the topological interactions between them play a crucial role [13, 14]. On the other hand, there has been an abundant production of heuristic rankings to identify influential nodes and "superspreaders" in networks [6–12, 19]. The main problem is that heuristic methods do not optimize a global function of influence. As a consequence, there is no guarantee of their performance.

Here we address the problem of quantifying node's influence by finding the optimal (i.e. minimal) set of structural influencers. After defining a unified mathematical framework for both immunization and spreading, we provide its optimal solution in random networks by mapping the problem onto optimal percolation. In addition, we present CI (which stands for Collective Influence), a scalable algorithm to solve the optimization problem in large scale datasets. The thorough comparison with competing methods (Methods Section I [20]) ultimately establishes the major performance of our algorithm. By taking into account collective influence effects, our optimization theory identifies a new class of strategic influencers, called weak-nodes, which outrank the hubs in the network. Thus, the top influencers are highly counterintuitive: low degree nodes play a major broker role in the network, and despite being weakly connected, can be powerful influencers.

The problem of finding the minimal set of activated nodes [17, 18] to spread information to the whole network [4] or to optimally immunize a network against epidemics [11] can be exactly mapped onto optimal percolation (see Methods Section II B). This mapping provides the mathematical support to the intuitive relation between influence and the concept of cohesion of a network: the most influential nodes are the ones forming the minimal set that guarantees a global connection of the network [5, 9, 10]. We call this minimal set the "optimal influencers" of the network. At a general level, the optimal influence problem can be stated as follows: find the minimal set of nodes which, if removed, would break down the network in many disconnected pieces. The natural measure of influence is, therefore, the size of the largest (giant) connected component as the influencers are removed from the network.

We consider a network composed of N nodes tied with M links with arbitrary degree distribution $P(k)$. Let us suppose we remove a certain fraction q of the total number

of nodes. It is well known from percolation theory [21] that, if we choose these nodes randomly, the network undergoes a structural collapse at a certain critical fraction where the probability of existence of the giant connected component vanishes, $G = 0$. The optimal influence problem corresponds to finding the minimum fraction q_c of influencers to fragment the network: $q_c = \min\{q \in [0, 1] : G(q) = 0\}$.

Let the vector $\mathbf{n} = (n_1, \dots, n_N)$ represents which node is removed ($n_i = 0$, influencer) or left ($n_i = 1$, the rest) in the network ($q = 1 - 1/N \sum_i n_i$), and consider a link from $i \rightarrow j$. The order parameter of the influence problem is the probability that i belongs to the giant component in a modified network where j is absent, $\nu_{i \rightarrow j}$ [22, 23]. Clearly, in the absence of a giant component we find $\{\nu_{i \rightarrow j} = 0\}$ for all $i \rightarrow j$. The stability of the solution $\{\nu_{i \rightarrow j} = 0\}$ is controlled by the largest eigenvalue $\lambda(\mathbf{n}; q)$ of the linear operator $\hat{\mathcal{M}}$ defined on the $2M \times 2M$ directed edges as $\mathcal{M}_{k \rightarrow \ell, i \rightarrow j} \equiv \left. \frac{\partial \nu_{i \rightarrow j}}{\partial \nu_{k \rightarrow \ell}} \right|_{\{\nu_{i \rightarrow j} = 0\}}$. We find for locally-tree like random graphs (see Fig. 1a and Methods Section II):

$$\mathcal{M}_{k \rightarrow \ell, i \rightarrow j} = n_i \mathcal{B}_{k \rightarrow \ell, i \rightarrow j} \quad (1)$$

where $\mathcal{B}_{k \rightarrow \ell, i \rightarrow j}$ is the *non-backtracking* matrix of the network [15, 24]. The matrix $\mathcal{B}_{k \rightarrow \ell, i \rightarrow j}$ has non-zero entries only when $(k \rightarrow \ell, i \rightarrow j)$ form a pair of consecutive non-backtracking directed edges, i.e. $(k \rightarrow \ell, \ell \rightarrow j)$ with $k \neq j$. In this case $\mathcal{B}_{k \rightarrow \ell, \ell \rightarrow j} = 1$ (Eq. S13). Powers of the matrix $\hat{\mathcal{B}}$ count the number of non-backtracking walks of a given length in the network (Fig. 1b) [24], much in the same way as powers of the adjacency matrix count the number of paths [5]. Operator $\hat{\mathcal{B}}$ has recently received a lot of attention thanks to its high performance in the problem of community detection [25, 26]. Below, we show its topological power in the problem of optimal percolation.

Stability of the solution $\{\nu_{i \rightarrow j} = 0\}$ requires $\lambda(\mathbf{n}; q) \leq 1$. The optimal influence problem for a given q ($\geq q_c$) can be rephrased as finding the optimal configuration \mathbf{n} that minimizes the largest eigenvalue $\lambda(\mathbf{n}; q)$ (Fig. 1c). The optimal set \mathbf{n}^* of Nq_c influencers is obtained when the minimum of the largest eigenvalue reaches the critical threshold:

$$\lambda(\mathbf{n}^*; q_c) = 1. \quad (2)$$

The formal mathematical mapping of the optimal influence problem to the minimization of the largest eigenvalue of the modified non-backtracking matrix for random networks, Eq. (2), represents our first main result.

An example of non-optimized solution corresponds to choosing n_i at random and decoupled from the non-backtracking matrix [23, 27] (random percolation [21], Methods Section IID). In the optimized case we seek to derandomize the selection of the set $n_i = 0$ and optimally choose them to find the best configuration \mathbf{n}^* with the lowest q_c according to Eq. (2). The eigenvalue $\lambda(\mathbf{n})$ (from now on we omit q in $\lambda(\mathbf{n}; q) \equiv \lambda(\mathbf{n})$, which is always kept fixed) determines the growth rate of an arbitrary vector \mathbf{w}_0 with $2M$ entries after ℓ iterations of the matrix $\hat{\mathcal{M}}$: $|\mathbf{w}_\ell(\mathbf{n})| = \langle \mathbf{w}_\ell | \mathbf{w}_\ell \rangle^{1/2} = |\hat{\mathcal{M}}^\ell \mathbf{w}_0| = \langle \mathbf{w}_0 | (\hat{\mathcal{M}}^\ell)^\dagger \hat{\mathcal{M}}^\ell | \mathbf{w}_0 \rangle^{1/2} \sim e^{\ell \log \lambda(\mathbf{n})}$. The largest eigenvalue is then calculated by the Power Method:

$$\lambda(\mathbf{n}) = \lim_{\ell \rightarrow \infty} \left[\frac{|\mathbf{w}_\ell(\mathbf{n})|}{|\mathbf{w}_0|} \right]^{1/\ell}. \quad (3)$$

Equation (3) is the starting point of an (infinite) perturbation series which provides the exact solution to the many-body influence problem in random networks and therefore contains all physical effects, including the collective influence. In practice, we minimize the cost energy function of influence $|\mathbf{w}_\ell(\mathbf{n})|$ in Eq. (3) for a finite ℓ . The solution rapidly converges to the exact value at $\ell \rightarrow \infty$; the faster the larger the spectral gap. We find for $\ell \geq 1$ as a leading order in $1/N$ (Methods Section IIE):

$$|\mathbf{w}_\ell(\mathbf{n})|^2 = \sum_{i=1}^N (k_i - 1) \sum_{j \in \partial \text{Ball}(i, 2\ell-1)} \left(\prod_{k \in \mathcal{P}_{2\ell-1}(i, j)} n_k \right) (k_j - 1), \quad (4)$$

where $\text{Ball}(i, \ell)$ is the set of nodes inside a ball of radius ℓ (defined as the shortest path) around node i , $\partial \text{Ball}(i, \ell)$ is the frontier of the ball and $\mathcal{P}_\ell(i, j)$ is the shortest path of length ℓ connecting i and j (Fig. 1d).

The first collective optimization in Eq. (4) is $\ell = 1$. We find $|\mathbf{w}_1(\mathbf{n})|^2 = \sum_{i, j=1}^N A_{ij} (k_i - 1)(k_j - 1)n_i n_j$ (Eq. S39). This term is interpreted as the energy of an antiferromagnetic Ising model with random bonds in a random external field at fixed magnetization, which is an example of a pair-wise NP-complete spin-glass whose solution is found in Methods Section III with the cavity method [28].

For $\ell \geq 2$, the problem can be mapped exactly to a statistical mechanical system with many-body interactions which can be recast in terms of a diagrammatic expansion, Eqs. S41-S49. For example, $|\mathbf{w}_2(\mathbf{n})|^2$ leads to 4-body interactions (Eq. S45), and, in general, the energy cost $|\mathbf{w}_\ell(\mathbf{n})|^2$ contains 2ℓ -body interactions. As soon as $\ell \geq 2$, the cavity method becomes much more complicated to implement and we use another suitable method, called

extremal optimization (EO) [29] (Methods Section IV). This method estimates the true optimal value of the threshold by finite size scaling following extrapolation to $\ell \rightarrow \infty$ (Extended Data Fig. 4). However, EO is not scalable to find the optimal configuration in large networks. Therefore, we develop an adaptive method, which performs excellently in practice, preserves the features of EO, and is highly scalable to present-day big-data.

The idea is to remove the nodes causing the biggest drop in the energy function Eq. (4). First, we define a ball of radius ℓ around every node (Fig. 1d). Then, we consider the nodes belonging to the frontier $\partial\text{Ball}(i, \ell)$ and assign to node i the collective influence (CI) strength at level ℓ following Eq. (4) (see Methods Section V for implementation and Section V A for minimizing $G(q) \neq 0$):

$$\text{CI}_\ell(i) = (k_i - 1) \sum_{j \in \partial\text{Ball}(i, \ell)} (k_j - 1) . \quad (5)$$

We notice that, while Eq. (4) is valid only for odd radii of the ball, $\text{CI}_\ell(i)$ is defined also for even radii. This generalization is possible by considering an energy function for even radii analogous to Eq. (4), as explained in Methods Section II G. The case of one-body interaction with zero radius $\ell = 0$ (Eq. S59) leads to the high-degree (HD) ranking (Eq. S62) [10].

The collective influence Eq. (5) is our second and most important result since it is the basis for the highly scalable and optimized CI-algorithm which follows. In the beginning all the nodes are present: $n_i = 1$ for all i . Then, we remove node i^* with highest CI_ℓ and set $n_{i^*} = 0$. The degrees of its neighbours are decreased by one, and the procedure is repeated to find the new top CI node to remove. The algorithm is terminated when the giant component is zero. By increasing the radius ℓ of the ball we obtain better and better approximations of the optimal exact solution at $\ell \rightarrow \infty$ (for finite networks, ℓ does not exceed the network diameter).

The collective influence CI_ℓ for $\ell \geq 1$ has a rich topological content, and consequently can tell us more about the role played by nodes in the network than the non-interacting high-degree hub removal strategy at $\ell = 0$, CI_0 . The augmented information comes from the sum in the r.h.s, which is absent in the naive high-degree rank. This sum contains the contribution of the nodes living on the surface of the ball surrounding the central vertex i , each node weighted by the factor $k_j - 1$. This means that a node placed at the center of a corona irradiating many links— the structure hierarchically emerging at different ℓ -levels as seen in Fig. 1e— can have a very large collective influence, even if it has a moderate or

low degree. Such “weak-nodes” can outrank nodes with larger degree that occupy mediocre peripheral locations in the network. The commonly used word ‘weak’ in this context sounds particularly paradoxical. It is, indeed, usually used as a synonym for a low-degree node with an additional “bridging” property, which has resisted a quantitative formulation. We provide this definition through Eq. (5), according to which weak nodes are, de facto, quite strong. Paraphrasing Granovetter’s conundrum [30], Eq. (5) quantifies the “strength of weak nodes”.

The CI-algorithm scales as $\sim O(N \log N)$ by removing a finite fraction of nodes at each step (Methods Section V B). This high scalability allows us to find top influencers in current big-data social media and optimal immunizers in large-scale populations at the country level. The applications are investigated next.

Figure 2a shows the optimal threshold q_c for random Erdős-Rényi (ER) network [5] (marked by the vertical line) obtained by extrapolating the EO solution to infinite size, $N \rightarrow \infty$, and $\ell \rightarrow \infty$ (Methods Section IV). In the same figure we compare the optimal threshold against the heuristic centrality measures: high-degree (HD) [9], high-degree adaptive (HDA), PageRank (PR) [7], closeness centrality (CC) [6], eigenvector centrality (EC) [6], and k-core [12] (see Methods Section I for definitions). Methods Section VI and VII show the comparison with the remaining heuristics [6, 11] and the Belief Propagation method of [14], respectively, which have worst computational complexity (and optimality), and cannot be applied to the network sizes used here. Remarkably, at the optimal value q_c predicted by our theory, the best among the heuristic methods (HDA, PR and HD) still predict a giant component $\sim 50\% - 60\%$ of the whole original network. Furthermore, the influencer threshold predicted by CI approximates very well the optimal one, and, notably, CI outperforms the other strategies. Figure 2b compares CI in scale-free (SF) network [5] against the best heuristic methods, i.e. HDA and HD. In all cases, CI produces smaller threshold and smaller giant component (Fig. 2c).

As an example of information spreading network, we consider the web of Twitter users (Methods Section VIII [19]). Figure 3a shows the giant component of Twitter when a fraction q of its influencers is removed following CI. It is surprising that a lot of Twitter users with a large number of contacts have a mild influence on the network, as witnessed by the fact that, when CI (at $\ell = 5$) predicts a zero giant component (and so it exhausts the number of optimal influencers), the scalable heuristic ranks (HD, HDA, PR and k-core) still give a

pretty big giant component of the order of 30-70% of the entire network, and, inevitably, find a remarkably larger number of (fake) influencers which is 50% larger than that predicted by CI (Fig. 3b and Methods Section VIII). One cause for the poor performance of the high-degree rank is that most of the hubs are clustered (rich-club effect), which gives a mediocre importance to their contacts. As a consequence, hubs are outranked by nodes with lower degree surrounded by coronas of hubs (shown in the detail of Fig. 3c), i.e. the weak-nodes predicted by the theory (Fig. 1e).

Finally, we simulate an immunization scheme on a personal contact network built on the phone calls performed by 14 million people in Mexico (Methods Section IX). Figure 3d shows that our method saves a large amount vaccines stockpile or, equivalently, find the smallest possible set of people to quarantine outranking the scalable heuristics in large real networks as well. Thus, while the mapping of the influencer identification problem onto optimal percolation is strictly valid for locally tree-like random networks, our results may apply also for real loopy networks, provided the density of loops is not excessively large.

Our solution to the optimal influence problem shows its importance in that it helps to unveil hitherto hidden relations between people, as witnessed by the weak-node effect. This, in turn, is the byproduct of a broader notion of influence, lifted from the individual non-interacting point of view [6–12, 19, 20] to the collective sphere: influence is an emergent property of collectivity and top influencers arise from the optimization of the complex interactions they stipulate.

-
- [1] Domingos P. & Richardson, M. Mining knowledge-sharing sites for viral marketing. *Proc. 8th ACM SIGKDD Intl. Conf. on Knowledge Discovery and Data Mining*, p61-70 (2002).
- [2] Pastor-Satorras R. &, Vespignani, A. Epidemic spreading in scale-free networks. *Phys. Rev. Lett.* **86**, 3200-3203 (2001).
- [3] Newman, M. E. J. Spread of epidemic disease on networks. *Phys. Rev. E* **66**, 016128 (2002).
- [4] Kempe, D., Kleinberg, J. & Tardos, E. Maximizing the spread of influence through a social network. *Proc. 9th ACM SIGKDD Intl. Conf. on Knowledge Discovery and Data Mining*, p137-143 (2003). doi: 10.1145/956750.956769
- [5] Newman, M. E. J. *Networks: An Introduction* (Oxford University Press, Oxford, 2010).
- [6] Freeman, L. C. Centrality in social networks: conceptual clarification. *Social Networks* **1**, 215-239 (1979).
- [7] Brin, S. & Page, L. The anatomy of a large-scale hypertextual web search engine. *Comput. Networks ISDN* **30**, 107-117 (1998).
- [8] Kleinberg, J. Authoritative sources in a hyperlinked environment. *Proc. 9th ACM-SIAM Symposium on Discrete Algorithms* (1998). Extended version in *J. of ACM* **46**, 604-632 (1999).
- [9] Albert, R., Jeong, H. & Barabási, A.-L. Error and attack tolerance of complex networks. *Nature* **406**, 378-382 (2000).
- [10] Cohen, R., Erez, K., ben-Avraham & D., Havlin, S. Breakdown of the Internet under intentional attack. *Phys. Rev. Lett.* **86**, 3682-3685 (2001).
- [11] Chen, Y., Paul, G., Havlin, S., Liljeros, F. & Stanley, H. E. Finding a better immunization strategy. *Phys. Rev. Lett.* **101**, 058701 (2008).
- [12] Kitsak, M., Gallos, L. K., Havlin, S., Liljeros, F., Muchnik, L., Stanley, H. E. & Makse, H. A. Identification of influential spreaders in complex networks. *Nature Phys.* **6**, 888-893 (2010).
- [13] Altarelli, F., Braunstein, A., Dall'Asta, L. & Zecchina, R. Optimizing spread dynamics on graphs by message passing. *J. Stat. Mech.* P09011 (2013).
- [14] Altarelli, F., Braunstein, A., Dall'Asta, L., Wakeling, J. R. & Zecchina, R. Containing epidemic outbreaks by message-passing techniques. *Phys. Rev. X* **4**, 021024 (2014).
- [15] Hashimoto, K. Zeta functions of finite graphs and representations of p-adic groups. *Adv. Stud. Pure Math.* **15**, 211-280 (1989).

- [16] Coja-Oghlan, A., Mossel, E. & Vilenchik, D. A spectral approach to analyzing Belief Propagation for 3-Coloring. *Combinatorics, Probability and Computing* **8**, 881-912 (2009).
- [17] Granovetter, M. Threshold models of collective behavior. *Am. J. Sociol.* **83**, 1420-1443 (1978).
- [18] Watts, D. J. A simple model of global cascades on random networks. *Proc. Natl. Acad. Sci. U.S.A.* **99**, 5766-5771 (2002).
- [19] Pei, S., Muchnik, L., Andrade, J. S. Jr., Zheng, Z. & Makse, H. A. Searching for superspreaders of information in real-world social media. *Sci. Rep.* **4**, 5547 (2014).
- [20] Pei, S. & Makse, H. A. Spreading dynamics in complex networks, *J. Stat. Mech.* P12002 (2013).
- [21] Bollobás, B. & Riordan, O. *Percolation* (Cambridge Univ. Press, Cambridge, 2006).
- [22] Bianconi, G. & Dorogovtsev, S. N. Multiple percolation transitions in a configuration model of network of networks. *Phys. Rev. E* **89**, 062814 (2014).
- [23] Karrer, B., Newman, M. E. J. & Zdeborová, L. Percolation on sparse networks. *Phys. Rev. Lett.* **113**, 208702 (2014).
- [24] Angel, O., Friedman, J. & Hoory, S. The non-backtracking spectrum of the universal cover of a graph. *Trans. Amer. Math. Soc.* **367** 4287-4318 (2015).
- [25] Krzakala, F., Moore, C., Mossel, E., Neeman, J., Sly, A., Zdeborová, L. & Zhang, P. Spectral redemption in clustering sparse networks. *Proc. Natl. Acad. Sci. U.S.A.* **110**, 20935-20940 (2013).
- [26] Newman, M. E. J. Spectral methods for community detection and graph partitioning. *Phys. Rev. E* **88**, 042822 (2013).
- [27] Radicchi, F. Predicting percolation thresholds in networks. *Phys. Rev. E* **91**, 010801(R) (2015).
- [28] Mézard, M. & Parisi, G. The cavity method at zero temperature. *J. Stat. Phys.* **111**, 1-34 (2003).
- [29] Boettcher, S. & Percus, A. G. Optimization with extremal dynamics. *Phys. Rev. Lett.* **86**, 5211-5214 (2001).
- [30] Granovetter, M. The strength of weak ties. *Am. J. Sociol.* **78**, 1360-1380 (1973).

Acknowledgments

This work was funded by NIH-NIGMS 1R21GM107641 and NSF-PoLS PHY-1305476. Additional support was provided by ARL. We thank L. Bo, S. Havlin and R. Mari for discussions and Grandata for providing the data on mobile phone calls.

Author contributions

Both authors contributed equally to the work presented in this paper.

Additional information

The authors declare no competing financial interests. Supplementary information accompanies this paper on www.nature.com/nature. Correspondence and requests for materials should be addressed to H.A.M. (hmakse@lev.cuny.cuny.edu).

FIG. 1. Non-backtracking (NB) matrix and weak-nodes. **a**, The largest eigenvalue λ of $\hat{\mathcal{M}}$ exemplified on a simple network. The optimal strategy for immunization and spreading minimizes λ by removing the minimum number of nodes (optimal influencers) that destroys all the loops. Left panel: The action of the matrix $\hat{\mathcal{M}}$ is on the directed edges of the network. The entry $\mathcal{M}_{2 \rightarrow 3, 3 \rightarrow 5} = n_3 \mathcal{B}_{2 \rightarrow 3, 3 \rightarrow 5} = n_3$ encodes node 3's occupancy ($n_3 = 1$) or vacancy ($n_3 = 0$). In this particular case, the largest eigenvalue is $\lambda = 1$. Center panel: Not-optimal removal of a leaf, $n_4 = 0$, which does not decrease λ . Right panel: Optimal removal of a loop, $n_3 = 0$, which decreases λ to zero. **b**, A NB walk is a random walk that is not allowed to return back along the edge that it just traversed. We show a NB open walk ($\ell = 3$), a NB closed walk with a tail ($\ell = 4$), and a NB closed walk with no tails ($\ell = 5$). The NB walks are the building blocks of the diagrammatic expansion to calculate λ . **c**, Representation of the global minimum over \mathbf{n} of the largest eigenvalue λ of $\hat{\mathcal{M}}$ vs q . When $q \geq q_c$, the minimum is at $\lambda = 0$. Then, $G = 0$ is stable (still, non-optimal configurations exist with $\lambda > 1$ for which $G > 0$). When $q < q_c$, the minimum of the largest eigenvalue is always $\lambda > 1$, the solution $G = 0$ is unstable, and then $G > 0$. At the optimal percolation transition, the minimum is at \mathbf{n}^* with $\lambda(\mathbf{n}^*, q_c) = 1$. For $q = 0$, we find $\lambda = \kappa - 1$ ($\kappa = \langle k^2 \rangle / \langle k \rangle$) which is the largest eigenvalue of $\hat{\mathcal{B}}$ for random networks [25] with all nodes present ($n_i = 1$). When $\lambda = 1$, the giant component is reduced to a tree plus one single loop (unicyclic graph), which is suddenly destroyed at the transition q_c to become a tree, causing the abrupt fall of λ to zero. **d**, $\text{Ball}(i, \ell)$ of radius ℓ around node i is the set of nodes contained in the grey region and ∂Ball is the set of nodes on the boundary. The shortest path from i to j is colored in red. **e**, Example of a weak-node: a node with a small number of connections surrounded by hierarchical coronas of hubs at different ℓ -levels.

FIG. 2. Exact optimal solution and performance of CI in synthetic networks. **a**, $G(q)$ in ER network ($N = 2 \times 10^5$, $\langle k \rangle = 3.5$, error bars are s.e.m. over 20 realizations) for the true optimal solution with EO (\times), CI, HDA, PR, HD, CC, EC and k-core. The other methods are not scalable and perform worst than HDA and are treated in Methods Sections VI and VII. CI is close to the optimal $q_c^{\text{opt}} \sim 0.193$ obtained with EO in Methods Section IV. Note that EO can estimate the extrapolated optimal value of q_c , but it cannot provide the optimal configuration for large systems. Inset: q_c (obtained at the peak of the second largest cluster) for the three best methods vs $\langle k \rangle$. **b**, $G(q)$ for SF network with degree exponent $\gamma = 3$, maximum degree $k_{\text{max}} = 10^3$ and $N = 2 \times 10^5$ (error bars are s.e.m. over 20

realizations). Inset: q_c vs γ . The continuous blue line is the HD analytical result computed in Methods Section II G. **c**, SF network with $\gamma = 3$ after the removal of the 15% of nodes, using the three methods. CI produces a much reduced giant component (red nodes).

FIG. 3. Performance of CI in large-scale real social networks. **a**, Giant component $G(q)$ of Twitter users [19] ($N = 469,013$) computed using CI, HDA, PR, PR and k-core strategies (other heuristics have prohibitive running times for this system size). **b**, Percentage of fake influencers or false positives (PFI, Eq. S120) in Twitter as a function of q , defined as the percentage of non-optimal influencers identified by HD algorithm in comparison with CI. Below q_c^{CI} , PFI reaches as much as $\sim 40\%$ indicating the failure of HD in optimally finding the top influencers. Indeed, to obtain $G = 0$, HD has to remove a much larger number of fake influencers, which at q_c^{HD} reaches PFI $\sim 48\%$. **c**, Example out of the many weak-nodes found in Twitter; the crucial influencer missed by all heuristic strategies. **d**, $G(q)$ for a social network of 1.4×10^7 mobile phone users in Mexico representing an example of big-data to test the scalability and performance of the algorithm. CI immunizes this social network using half a million less people than the best heuristic strategy (HDA), saving $\sim 35\%$ of vaccine stockpile.

Extended Data Fig. 1. HD high-degree threshold. **a**, HD influence threshold q_c as a function of the degree distribution exponent γ of scale-free networks in the ensemble with $k_{\max} = mN^{1/(\gamma-1)}$ and $N \rightarrow \infty$. The curves refer to different values of the minimum degree m : 1 (red), 2 (blue), 3 (black). The fragility of SF networks (small q_c) is notable for $m = 1$, the case calculated in [10]. In this case, the network contains many leaves, and reduces to a star at $\gamma = 2$ which is trivially destroyed by removing the only single hub, explaining the general fragility in this case. Furthermore, in this case, the network becomes a collection of dimers with $k = 1$ when $\gamma \rightarrow \infty$, which is still trivially fragile. This explains why $q_c \rightarrow 0$ as $\gamma \rightarrow \infty$, as well. Therefore, the fragility in the case $m = 1$ has its roots in these two limiting trivial cases. Removing the leaves ($m = 2$) results in a 2-core, which is already more robust. For the 3-core $m = 3$, $q_c \approx 0.4 - 0.5$ provides a quite robust network, and has the expected asymptotic limit to a non-zero q_c of a random regular graph with $k = 3$ as $\gamma \rightarrow \infty$, $q_c \rightarrow (k - 2)/(k - 1) = 0.5$. Thus, SF networks become robust in these more realistic cases and the search for other attack strategies becomes even more important.

b, HD influence threshold q_c as a function of the degree distribution exponent of scale-free networks with minimum degree $m = 2$ in the ensemble where k_{\max} is fixed and does not scale with N . The curves refer to different values of the cut-off k_{\max} : 10^2 (red), 10^3 (green), 10^5 (blue), 10^8 (magenta), and $k_{\max} = \infty$ (black), and show that for typical k_{\max} degree of 10^3 , for instance in social networks, the network is fairly robust with $q_c \approx 0.2$ for all γ .

Extended Data Fig. 2. RS estimation of the maximum eigenvalue. Main panel: the eigenvalue $\lambda_1^{\text{RS}}(q)$ obtained by minimizing the energy function $\mathcal{E}(\mathbf{s})$ with the RS cavity method. The curve was computed on a Erdős-Rényi graph of $N = 10,000$ nodes and average degree $\langle k \rangle = 3.5$ and then averaged over 40 realizations of the network. Inset: Comparison between the cavity method and extremal optimization for an ER graph of $\langle k \rangle = 3.5$ and $N = 128$. The curves are averaged over 200 realizations (error bars are s.e.m.).

Extended Data Fig. 3. EO estimation of the maximum eigenvalue. Eigenvalue $\lambda(q)$ obtained by minimizing the energy function $\mathcal{E}(\mathbf{n})$ with τ EO, plotted as a function of the fraction of removed nodes q . The panels are for different orders of the interactions. The curves in each panel refer to different sizes of Erdős-Rényi networks with average connectivity $\langle k \rangle = 3.5$. Each curve is an average over 200 instances (error bars are s.e.m.). The value q_c where $\lambda(q_c) = 1$ is the threshold for a particular N and many-body interaction.

Extended Data Fig. 4. Estimation of optimal threshold q_c^{opt} with EO. **a**, Critical

threshold q_c as a function of the system size N obtained with EO from Extended Data Fig. 3 of ER networks with $\langle k \rangle = 3.5$ and varying size. The curves refer to different orders of the many-body interactions. The data show a linear behaviour as a function of $N^{-2/3}$, typical of spin glasses, for each many-body interaction ρ . The extrapolated value $q_c^\infty(\rho)$ is obtained at the y -intercept. **b**, Thermodynamical critical threshold $q_c^\infty(\rho)$ as a function of the order of the interactions ρ from **a**. The data scale linearly with $1/\rho$. From the y -intercept of the linear fit we obtain the thermodynamical limit of the infinite-body optimal value $q_c^{\text{opt}} = q_c^\infty(\rho \rightarrow \infty) = 0.192(9)$.

Extended Data 5. Comparison of the CI algorithm for different radius ℓ of the Ball(ℓ). We use $\ell = 1, 2, 3, 4, 5$, on a ER graph with average degree $\langle k \rangle = 3.5$ and $N = 10^5$ (the average is taken over 20 realizations of the network, error bars are s.e.m.). For $\ell = 3$ the performance is already practically indistinguishable from $\ell = 4, 5$. The stability analysis we developed to minimize q_c is strictly valid only when $G = 0$, since the largest eigenvalue of the modified NB matrix controls the stability of the solution $G = 0$, and not the stability of the solution $G > 0$. In the region where $G > 0$ we use a simple and fast procedure to minimize G explained in Section V A. This explains why there is a small dependence on ℓ having a slightly larger G for larger ℓ , when $G > 0$ in the region $q \approx 0.15$.

Extended Data Fig. 6. Illustration of the algorithm used to minimize $G(q)$ for $q < q_c$. Starting from the completely fragmented network at $q = q_c$, nodes are reinserted with the following criterion: each node is assigned an index $c(i)$ given by the number of clusters it would join if it were reinserted in the network. For example, the red node has $c(\text{red}) = 2$, while the blue one has $c(\text{blue}) = 3$. The node with the smallest $c(i)$ is reinserted in the network: in this case the red node. Then the $c(i)$'s are recalculated and the new node with the smallest $c(i)$ is found and reinserted. The algorithm is repeated until all the removed nodes are reinserted in the network.

Extended Data Fig. 7. Test of the decimation fraction. Giant component as a function of the removed nodes using CI, for an ER network of $N = 10^5$ nodes and average degree $\langle k \rangle = 3.5$. The profiles of the curves are drawn for different percentages of nodes fixed at each step of the decimation algorithm.

Extended Data Fig. 8. Comparison of the performance of CI, BC, and EGP. We also include HD, HDA, EC, CC, k-core, and PR. We use a scale-free network with degree exponent $\gamma = 2.5$, average degree $\langle k \rangle = 4.68$, and $N = 10^4$. We use the same parameters as

in Ref. [11].

Extended Data Fig. 9. Comparison with BP. **a**, Fraction of infected nodes f as a function of the fraction of immunized nodes q in SIR from BP solution. We use a ER random graph of $N = 200$ nodes and average degree $\langle k \rangle = 3.5$. The fraction of initially infected nodes is $p = 0.1$ and the inverse temperature $\beta = 3.0$. The profiles are drawn for different values of the transmission probability w : 0.4 (red curve), 0.5 (green), 0.6 (blue), 0.7 (magenta). Also shown are the results of the fixed density BP algorithm (open circles). **b**, Chemical potential μ as a function of the immunized nodes q from BP. We use a ER random graph of $N = 200$ nodes and average degree $\langle k \rangle = 3.5$. The fraction of the initially infected nodes is $p = 0.1$ and the inverse temperature $\beta = 3.0$. The profiles are drawn for different values of the transmission probability w : 0.4 (red curve), 0.5 (green), 0.6 (blue), 0.7 (magenta). Also shown are the results of the fixed density BP algorithm (open circles) for the region where the chemical potential is non convex. **c**, Comparison between the giant components obtained with CI, HDA, HD and BP. We use an ER network of $N = 10^3$ and $\langle k \rangle = 3.5$. We also show the solution of CI from Fig. 2a for $N = 10^5$. We find in order of performance: CI, HDA, BP, and HD. (The average is taken over 20 realizations of the network, error bars are s.e.m.) **d**, Comparison between the giant components obtained with CI, HDA, HD and BPD. We use a SF network with degree exponent $\gamma = 3.0$, minimum degree $k_{\min} = 2$, and $N = 10^4$ nodes.

Extended Data Fig. 10. Fraction of infected nodes $f(q)$ as a function of the fraction of immunized nodes q in SIR from BP. We use the following parameters: initial infected people $p = 0.1$, and transmission probability $w = 0.5$. We use an ER network of $N = 10^3$ nodes and $\langle k \rangle = 3.5$. We compare CI, HDA and BP. All strategies give similar performance due to the large value of the initial infection p which washes out the optimization performed by any sensible strategy, in agreement with the results of [14], Fig 12a.

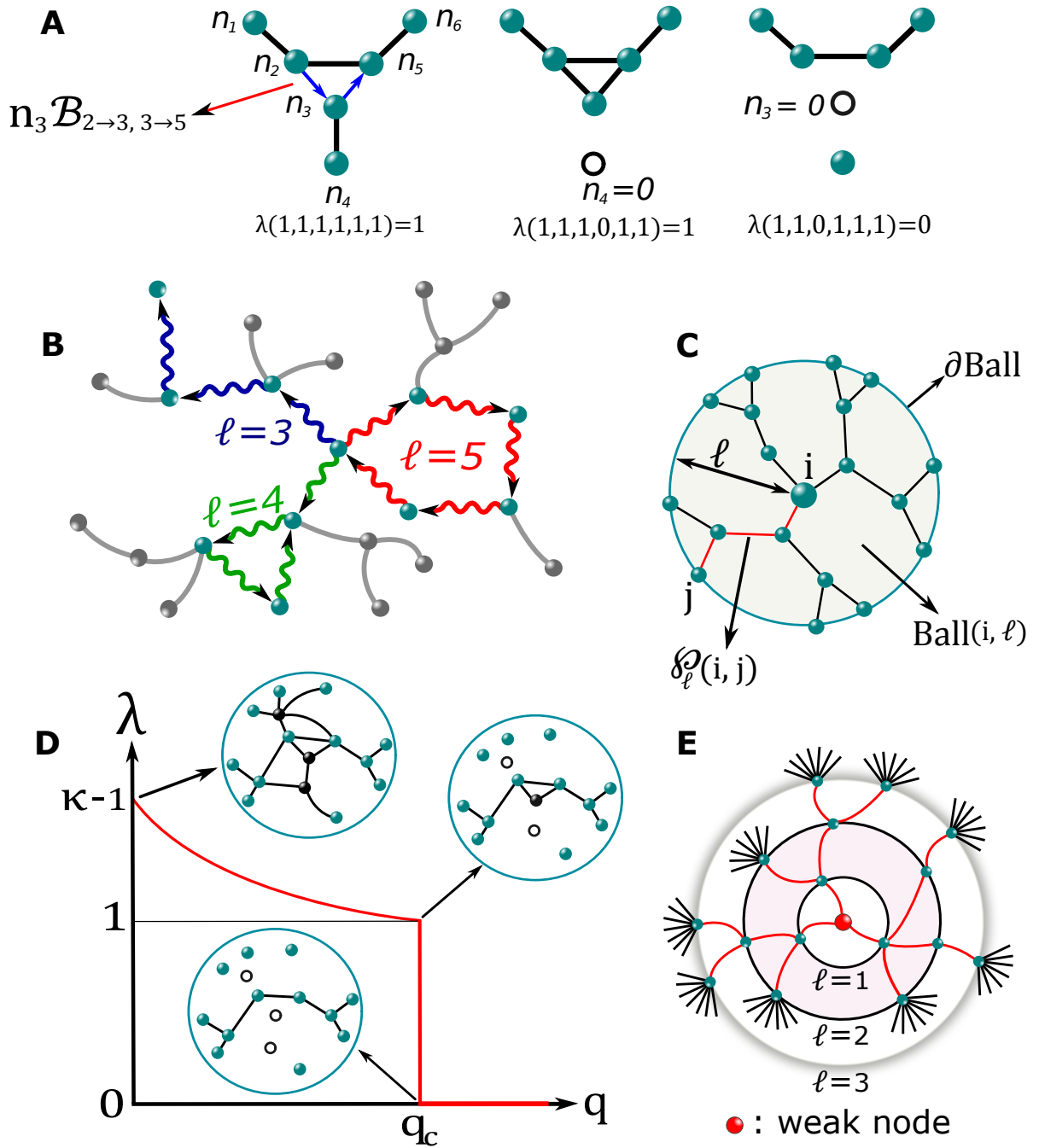


FIG. 1.

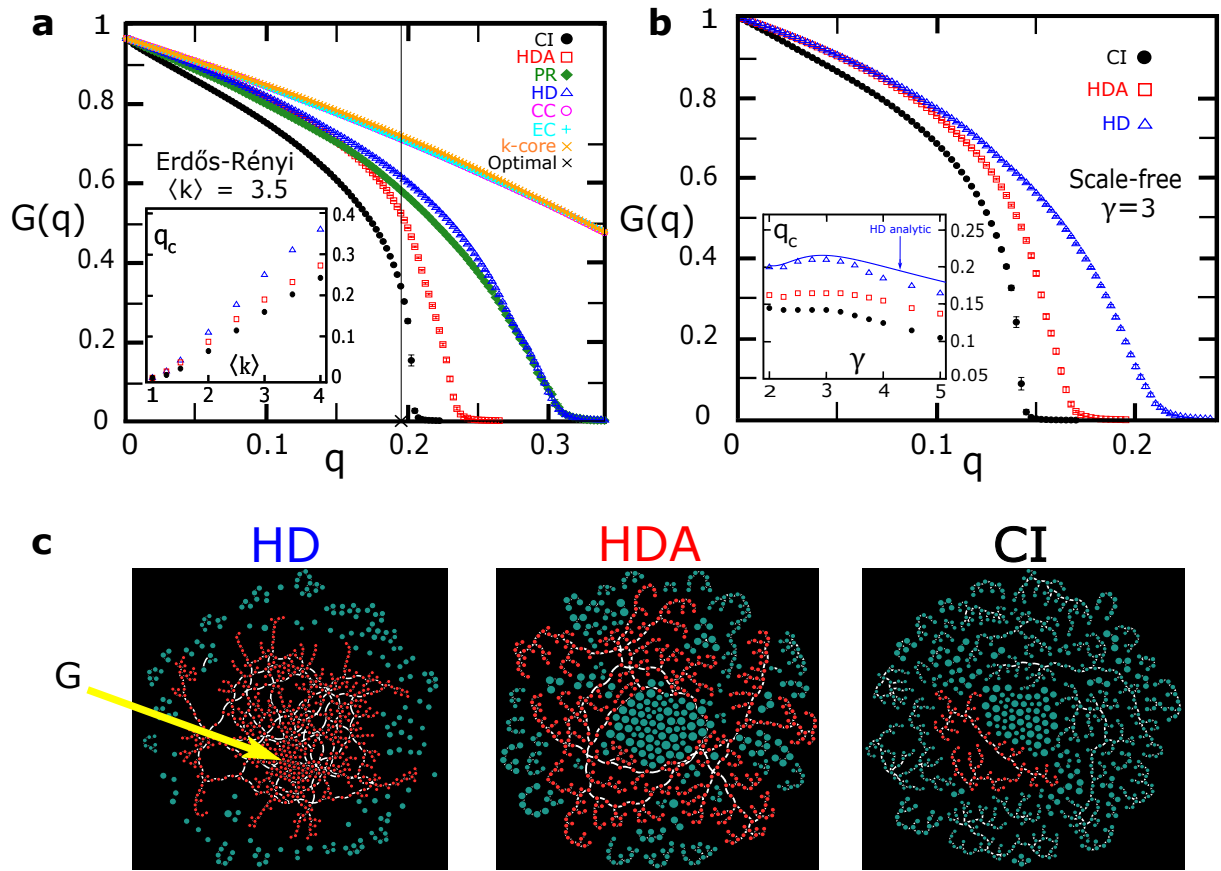


FIG. 2.

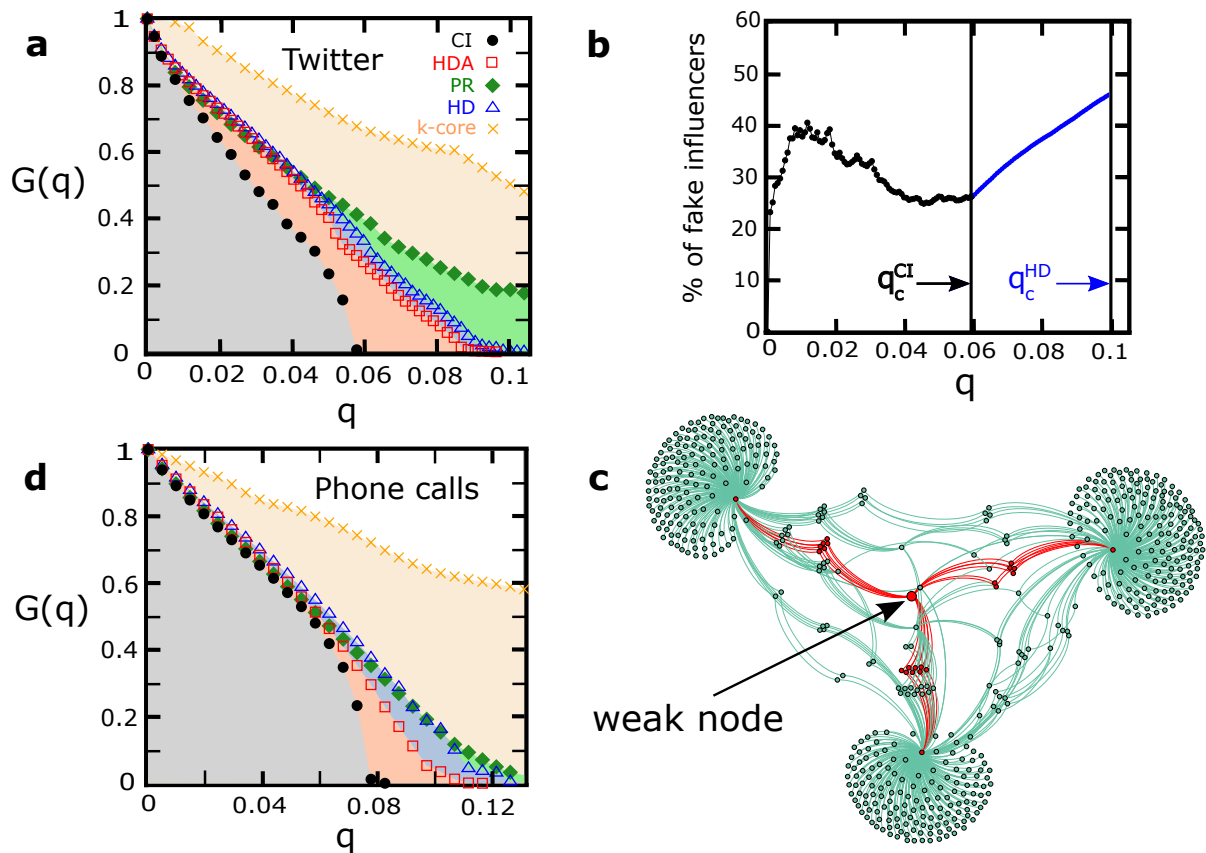


FIG. 3.

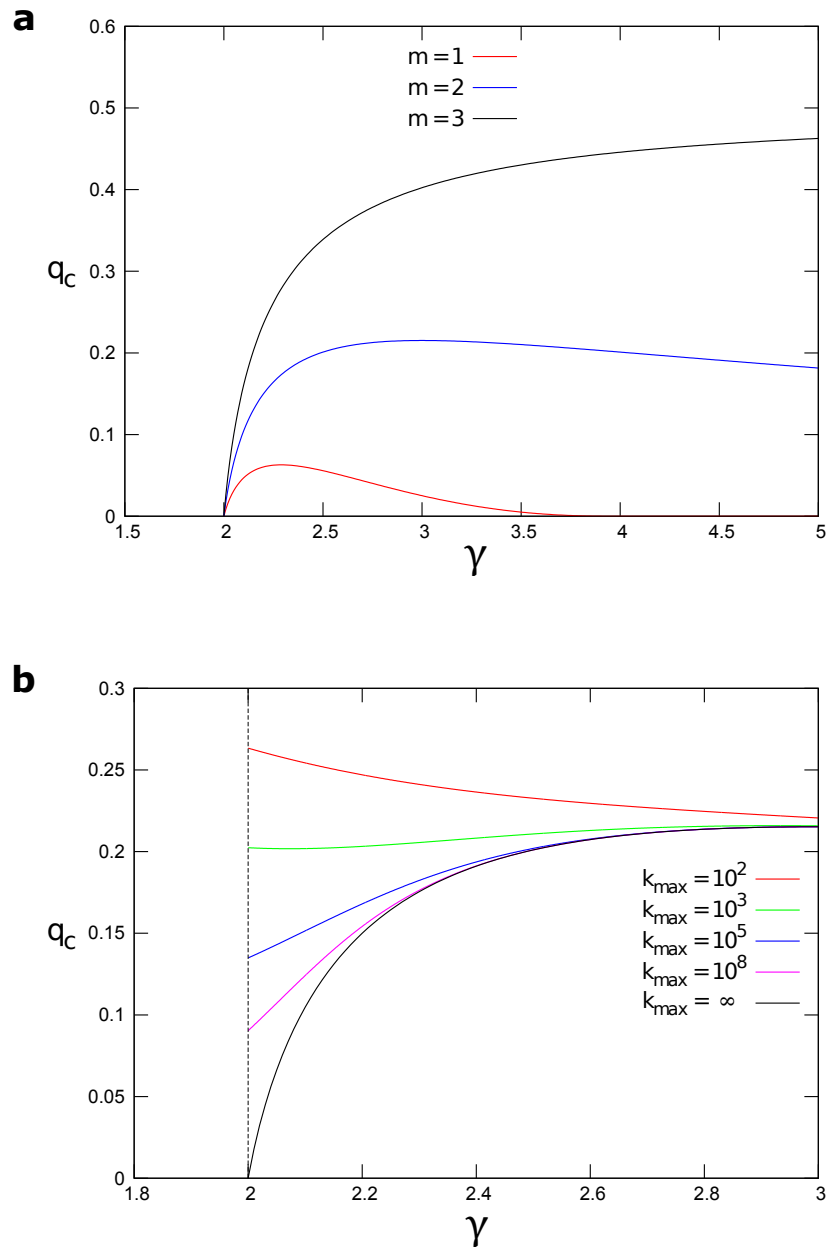


FIG. 1. Extended Data

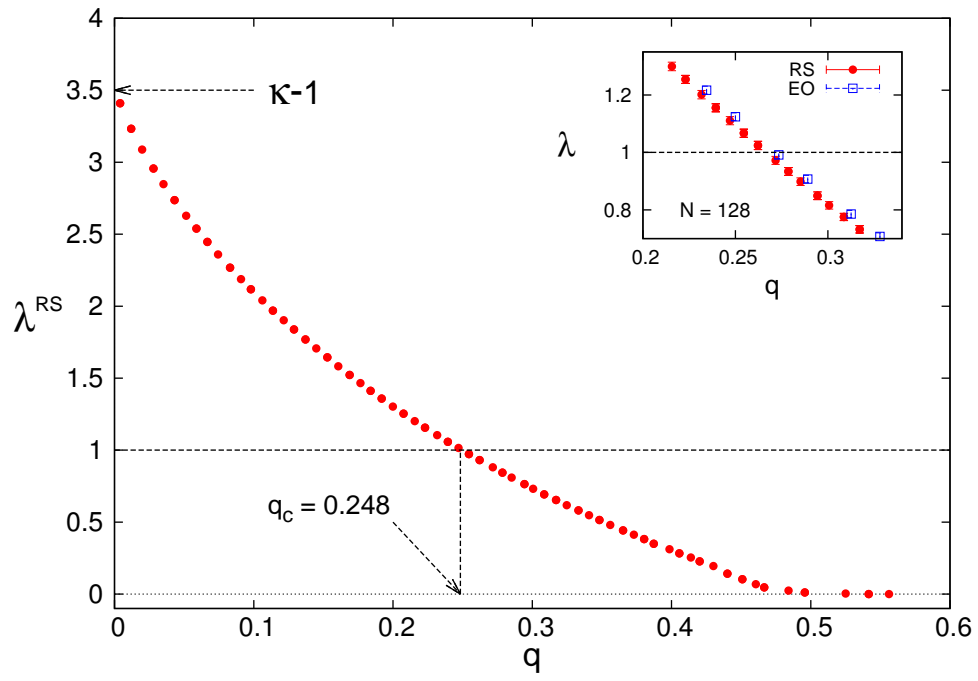


FIG. 2. Extended Data

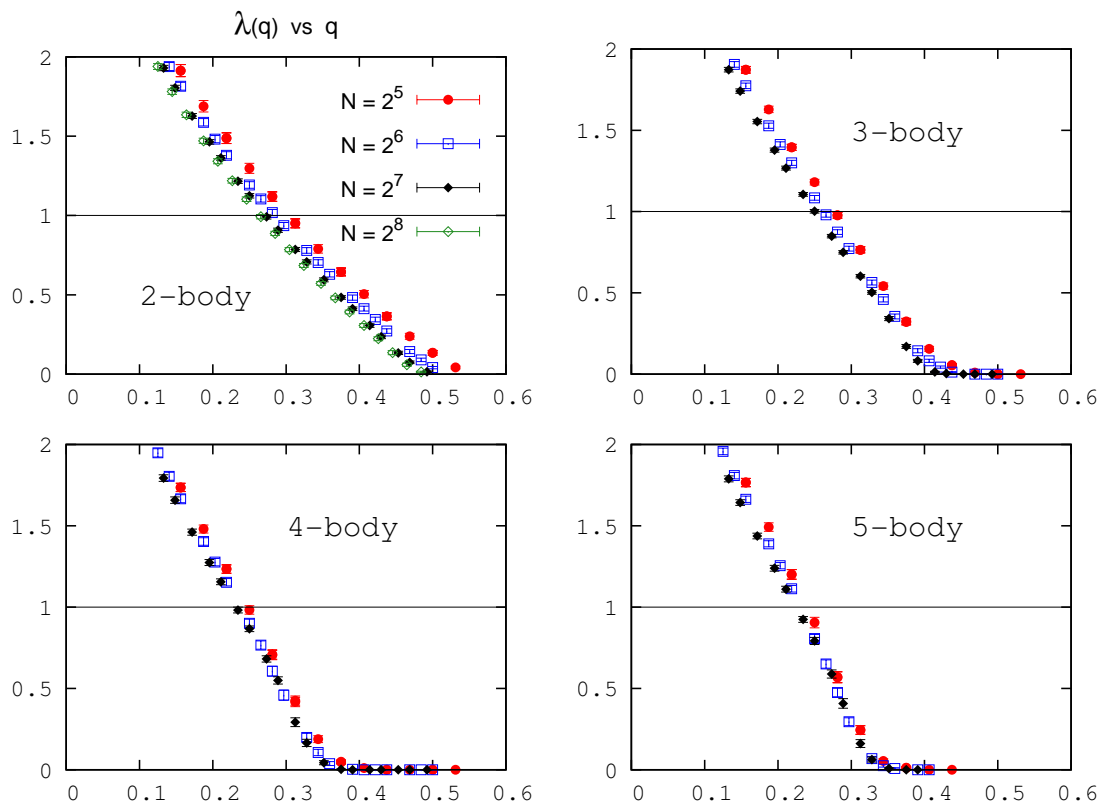


FIG. 3. Extended Data

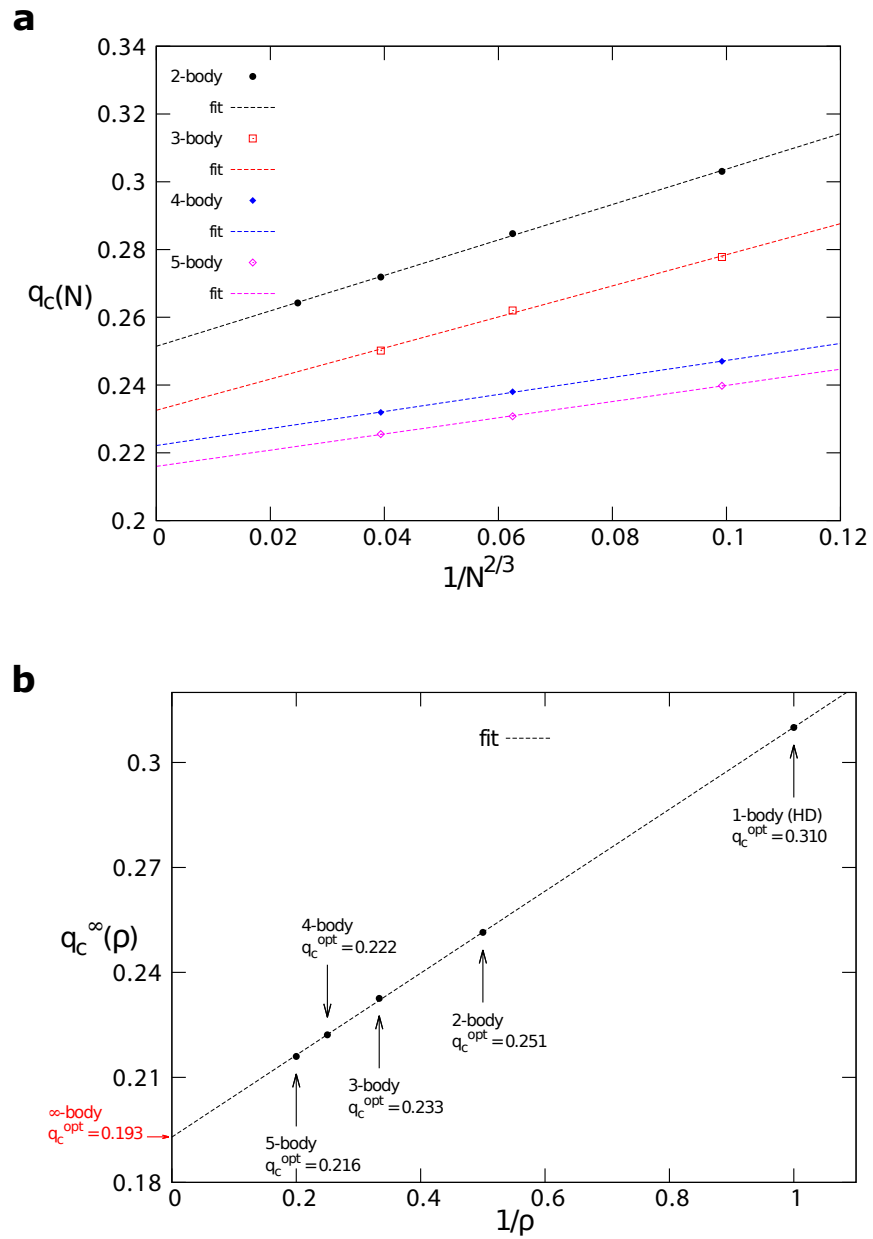


FIG. 4. Extended Data

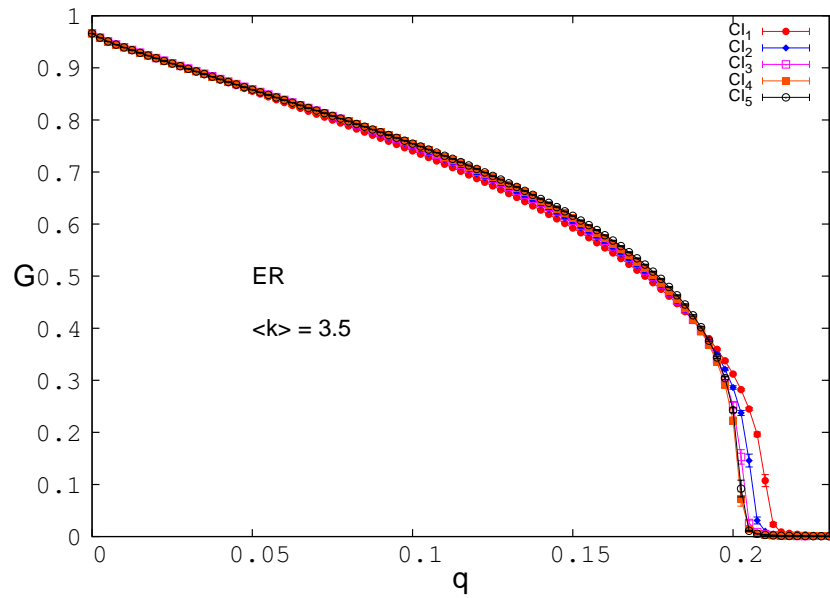


FIG. 5. Extended Data

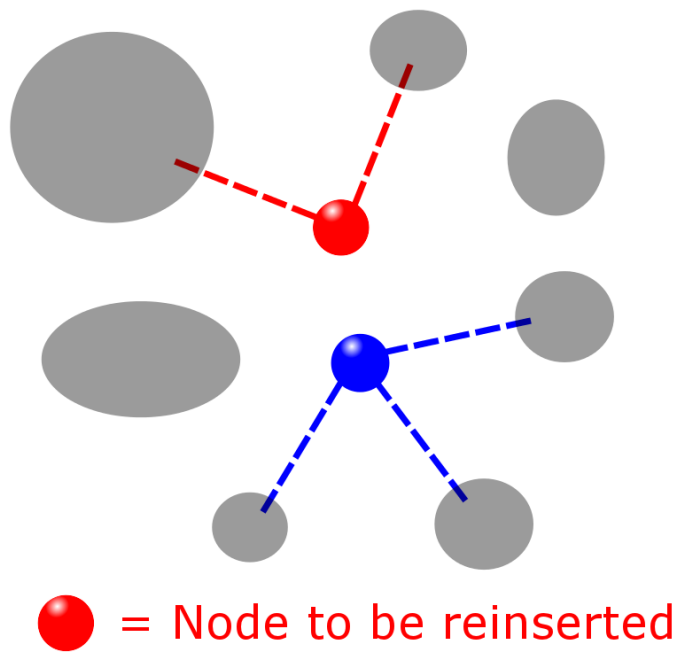


FIG. 6. Extended Data

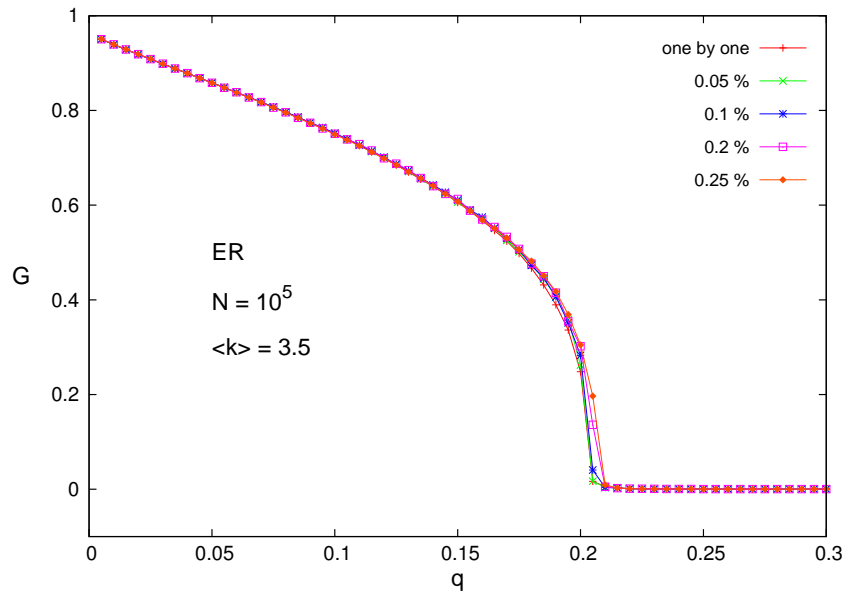


FIG. 7. Extended Data

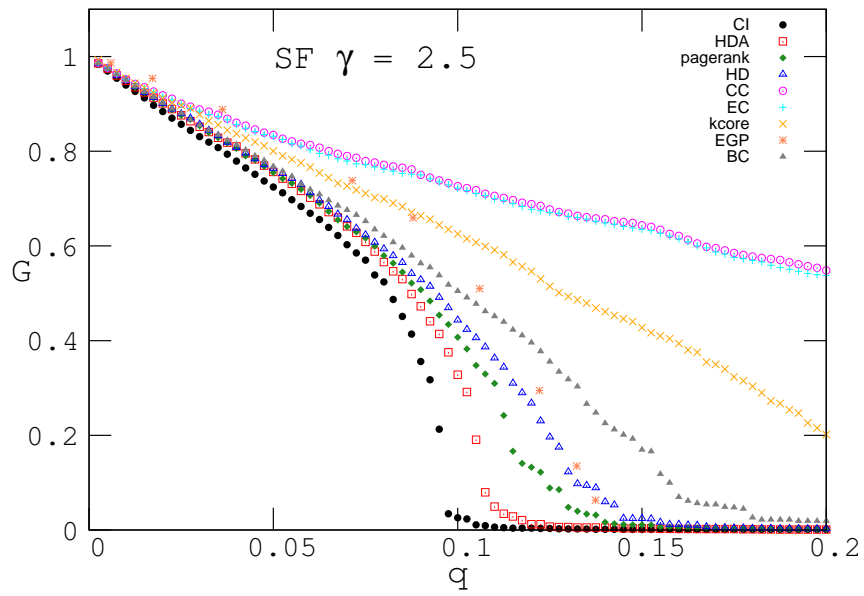


FIG. 8. Extended Data

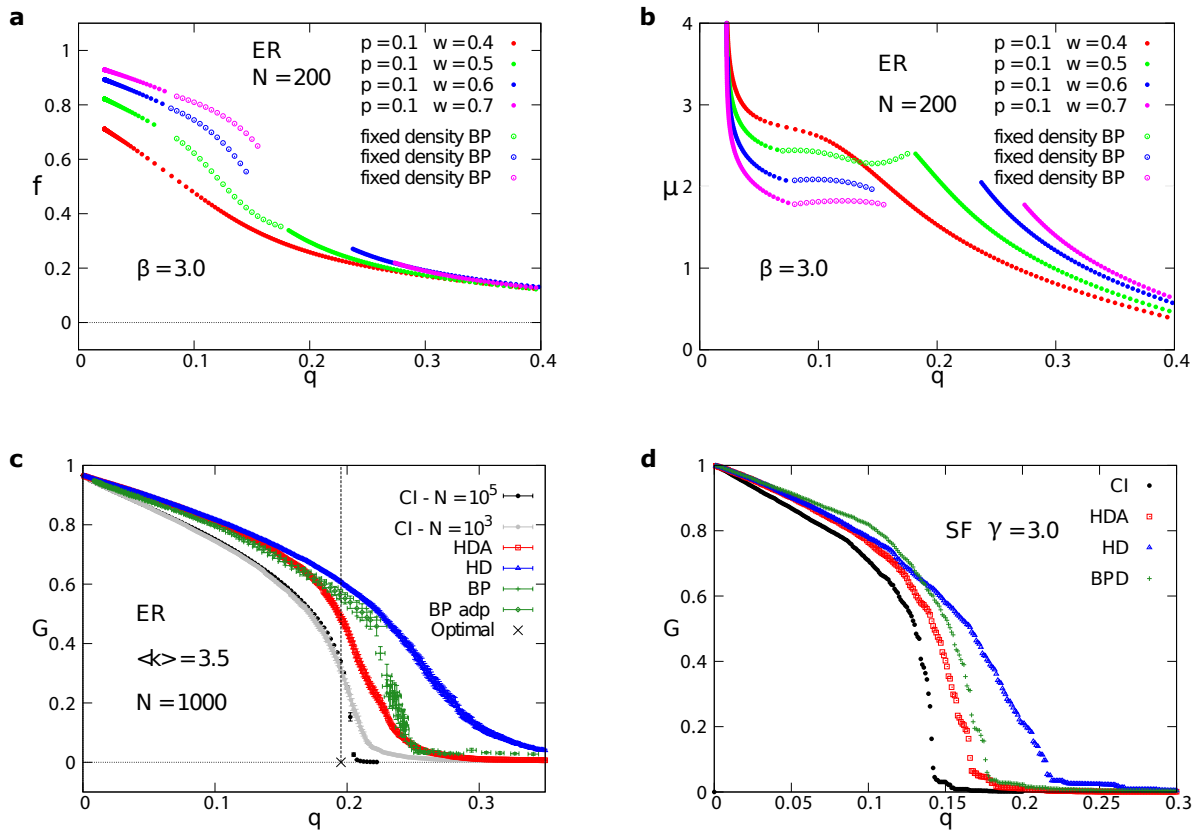


FIG. 9. Extended Data

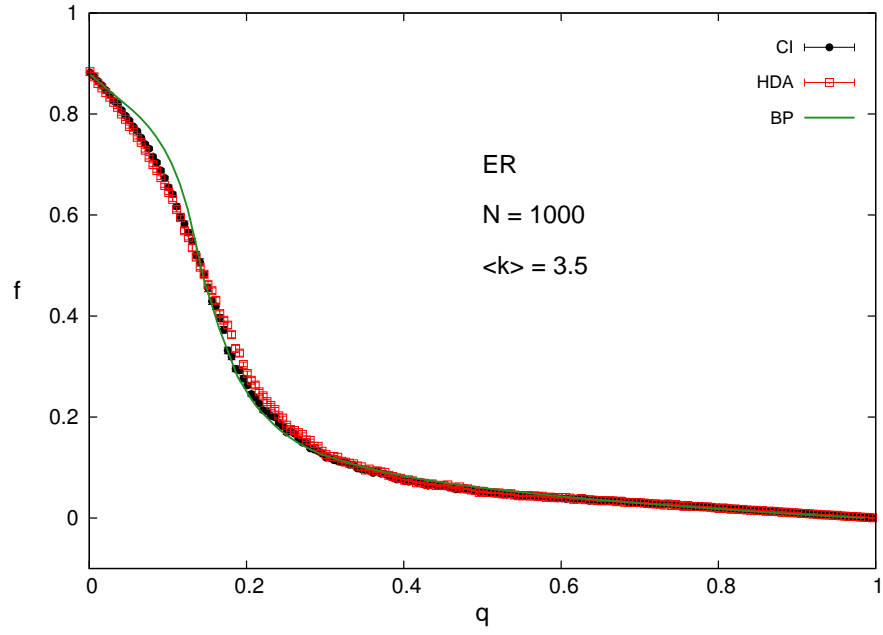


FIG. 10. Extended Data

METHODS

Influence maximization in complex networks through optimal percolation

Flaviano Morone & Hernán A. Makse

CONTENTS

References	8
I. Heuristic methods used to identify influential spreaders in complex networks	29
II. Collective Theory of Optimal Influence	31
A. Optimal Percolation	33
B. Mapping of optimal immunization and spreading problems onto optimal percolation	38
C. Limit of applicability of the theory of influence	41
D. Random influence	42
E. Derivation of the main formula: cost energy function of influence, Eq. (4)	43
F. Interpretation in terms of NB walks and generalization to 2ℓ -body interactions	47
G. Odd $(2\ell + 1)$ -body interactions	50
H. HD attack at $\ell = 0$ one-body problem	50
III. Optimization with the Cavity Method	53
IV. Minimization with Extremal Optimization (EO)	59
A. τ -EO with multibody interactions	62
V. CI Algorithm	64
A. Optimization for $G(q) \neq 0$	65
B. Scalability of the CI algorithm	68
C. Effect of the percentage of fixed nodes during adaptive CI	68
VI. Comparison with other heuristic methods	69
VII. Comparison with Belief Propagation algorithm of Altarelli <i>et al.</i> [14]	69
A. BP adaptive	73

B. Comparison	74
1. First comparison	74
2. Second comparison	75
VIII. A new paradigm of influence in social media: Twitter	78
IX. Halting epidemics: Mobile phone call network	80
References	81

I. HEURISTIC METHODS USED TO IDENTIFY INFLUENTIAL SPREADERS IN COMPLEX NETWORKS

In this section we describe the existing heuristic algorithms in the literature that have been used to identify influential spreaders and superspreaders in networks. We use these heuristics to compare with our collective theory of influence. A common feature of the heuristic methods is that they are not designed from first principles and therefore do not necessarily optimize an influence measure. Instead, they are based on intuitive ideas about what is an influencer. Besides, the heuristics constitute ranking of nodes lacking the collective influence arising from considering all the influencers at once. On the other hand, the theoretical framework for maximizing the spread of influence of Kempe *et al.* [4] and the Belief Propagation theory for the optimal immunization problem of Altarelli *et al.* [14, 48] contain the necessary optimization of influence. The greedy algorithm considered in [4] has prohibitive running time for all the networks considered in our work. Detailed comparison with the Belief Propagation is done in Methods Section VII.

High-Degree (HD) [2, 9, 10]. In the HD method nodes are ranked by degree, and sequentially removed starting from the node of highest degree. One of the limitations of this method is the fact that hubs may form tightly-knit groups called “rich-clubs” [31, 32]. Strategies based on high-degree will highly rank these rich-club hubs. On the other hand, an optimized scheme will target only one of them to avoid overlap between the already attacked areas in the network. **High Degree Adaptive (HDA)** is the adaptive version where the degree of the remaining nodes is recomputed after each node removal.

PageRank (PR) [7]. This is the famous Google’s algorithm for ranking websites. It was proposed for first time in [7] to “condensing every page in the World Wide Web into a single number, its PageRank. PageRank is a global ranking of all web pages, regardless of their content, based solely on their location in the Web’s graph structure.” PR can be thought of as the most successful rank, ever. At its heart, it is another eigenvector centrality. It computes the probability that, if someone follows links on the web at random, performing a random walk of clicks, he/she eventually hits your website. The higher this chance, the higher the PR of the website. Therefore, sites that get linked more are considered reputable, and, linking to other websites, they pass that reputation along. Thus, the shortcoming with PR comes from the fact that PR takes node’s score into account when calculating other’s

scores. In other words, a high-PR site may confer a much higher score to otherwise unpopular sites it happens to link. Notice that in our algorithm using the non-backtracking operator this problem is cured nicely, since the influence is computed by "ignoring" the node you come from.

K-core [12]. K-core ranking is based on the k-shell decomposition of the network. Each node is assigned the k-shell number, k_S , i.e. the order of the shell it belongs to. In k-shell decomposition, we first remove all nodes with degree $k = 1$ and continue pruning the network iteratively until there is no node with $k = 1$. These removed nodes belong to the peripheric k-shell with index $k_S = 1$. Similarly, the next k-shells are defined until all nodes are pruned and we get to the kcore of the network. The rank based on kcore produces good results in identifying single spreaders individually, but has a poor performance for multiple spreaders (the case considered in the present manuscript), because putting spreaders in the same k-shell gives a marginal or null advantage, as recognized in [12]. That is, ranking the spreaders one by one, one may find that the best of them are located in the core. However, when considering the maximization of influence of all spreaders at the same time, collective effects coming from interactions between the spreaders via overlap of their spheres of influence are crucial: even if the top spreader is in the core, the next spreader most probably will not be in the core, because the core is already infected by the first spreader. Indeed, these interactions between spreaders are what makes the problem hard to solve (NP-hard as shown in [4]). Thus, even if the best individually-ranked spreaders might be located in the kcore, their collective influence is determined by their full set of interactions. Therefore, for multiple spreaders, the kshell ranking is not optimal, although, choosing core nodes separated by a distance increases their optimality as already shown in [12].

Eigenvector Centrality (EC) [33]. It is the eigenvector corresponding to the largest eigenvalue of the adjacency matrix. Node rank is the corresponding entry of the eigenvector. Nodes are removed starting from the highest rank. This method is not very powerful, especially for the case of SF networks, where most of the weight may be carried by few nodes (hubs), while the others have vanishingly small weights, and thus they are not properly ranked.

Closeness Centrality (CC) [34]. Closeness centrality measures how close a vertex is to all other vertices in the graph. More precisely CC at node i is the inverse of the average distance to all other nodes. Nodes are ranked according to their CC from the highest to

the lowest score, and removed accordingly. A property of CC is that it tends to give high scores to individuals who are near the center of local clusters (i.e. network communities), and hence it over-allocates spreaders (or immunized nodes) next to each other. Moreover, it comes with a high computational cost that prevents the application to large networks.

Methods Section VI compares results with **betweenness centrality** [35] and **equal-graph-partitioning** [11] which present prohibitive running times for the large-scale networks used here and present worst performance than other heuristics.

II. COLLECTIVE THEORY OF OPTIMAL INFLUENCE

Nodes forming complex networks play different roles, depending on the process in which they participate [5]. Their inherent strength and weakness emerge collectively from the pattern of interactions with the other components. Nonetheless, it is a common practice to quantify node’s importance in a network [5, 8], for example social rank order [32], by individual node’s attributes such as the amount of its connections [2, 9, 10], betweenness and eigenvector centralities [6], or its closeness to the core [12]. This attitude is, nowadays, amplified by the augmented reality provided by virtual social networks. This idea has also permeated to other fields and it is common to strategies of immunization [2, 11], viral spreading of information and marketing in social media [1, 19], as well as targeted attack schemes to infrastructure networks [9, 10]. However, individual node ranking is an ambiguous definition of node’s influence, for it considers the influencers as isolated entities and not in interaction with each other. Yet, there has been an abundant production on the subject of identifying most influential nodes and ”superspreaders” using such rankings [6, 7, 9–12, 19, 20]. The main problem is that all these methods do not optimize an objective global function of influence. Instead, they are based on assumptions about the importance of individual properties of the node [20] and, inevitably, they fail to take into account the collective influence of the whole set of nodes. As a consequence, there is no guarantee of their performance.

On the other hand, a theoretical framework taking into account a global maximization of influence was outlined by Kempe *et al.* [4] in the form of a discrete global optimization problem for diffusion of information models such as the Linear Threshold Model (LTM) of Granovetter [17] and other variants [18], whose solution is proved to be NP-hard and is

approximated by a greedy algorithm [4]. This approach makes leverage on a special attribute of the function of influence to be optimized, called submodularity, which express the decrease in the gain in the output of the process after an increment of the input factors. This "diminishing return" property is often lost in many optimization problems. In particular, submodularity does not apply, in general, to the giant connected component in optimal percolation problem, which is the function we minimize. It should be said that for some LTMs, of the type treated in [4], the objective function of influence to be maximized can be proven to be submodular. However, this does not hold true in general for other classes of LTMs, for example in the case of a fixed choice of the thresholds, as explicitly stated in [4], and which represents the type of problem studied in this paper. As a consequence even the greedy algorithm does not provide a stable approximation to the optimal solution. Furthermore, greedy searches are not scalable and therefore not applicable to current day big data in social media and population immunization problems. In our case we face these difficulties.

Another pioneering approach to the problem of influence optimization and immunization is outlined in Refs. [13, 14]. In particular, in Ref. [14], the authors use a very interesting and principled method, based on Belief Propagation (BP), to minimize the expected infection outbreak in an epidemic process (modeled as susceptible-infected-recovered, SIR, or susceptible-infected-susceptible, SIS) for a given number of immunized nodes, and for a given choice of the parameters of the model, i.e., transmission probability w and initial fraction of infected individuals, p . While the method is able to find nearly optimal solutions to the problem, it becomes unfeasible when $p \rightarrow 0$, which corresponds to the optimal influence problem treated here, because the time complexity of the algorithm diverges as p^{-3} for $p \rightarrow 0$. A full comparison between our theory and BP is performed in Methods Section VII.

From the theoretical standpoint, our main result is the discovery of a method to map the problem of optimal influence onto the computation of the minimal set of nodes that minimizes the largest eigenvalue of the Non-Backtracking matrix of the network. This operator has recently received a lot of attention thanks to its high performance in the problem of community detection [25, 26]. We show its formidable topological power in the problem of optimal influence. The problem we set up is, in its most general formulation, intractably hard. We present a perturbative solution along with a very fast algorithm, that we use to simulate an optimized immunization/quarantine and superspreading protocol on

very large real networks. The naive strategy, corresponding to the lowest approximation, is given by the attack on the high degree nodes. The first non-trivial attack strategy is equivalent to find the ground state of a spin-glass like system, i.e., an anti-ferromagnetic Ising model with random bonds in a random external field at fixed magnetization. Higher order approximations produce superior performance compared to previous heuristic strategies. Furthermore, the algorithm is highly scalable with running time $O(N \log N)$.

A. Optimal Percolation

A network is a set of N nodes tied together by M edges. The vector $\mathbf{n} = (n_1, \dots, n_N)$ represents which node is present and which one is removed. We adopt the convention that $n_i = 1$ if node i is present, and $n_i = 0$ if node i is removed (corresponding to an influencer). The total fraction of removed nodes is denoted with q :

$$q = 1 - \frac{1}{N} \sum_{i=1}^N n_i \equiv 1 - \langle n \rangle . \quad (6)$$

We call $G(q)$ the fraction of occupied sites belonging to the giant (largest) connected component (in the limit $N \rightarrow \infty$ represents the probability of existence of the giant component). The optimal percolation problem is finding the minimum fraction q_c of nodes to be removed such that $G(q_c) = 0$:

$$q_c = \min\{q \in [0, 1] : G(q) = 0\} . \quad (7)$$

For $q \geq q_c$, the network consists of a collection of clusters of nodes whose sizes are subextensive. Alternatively, for a fixed fraction $q < q_c$, we search for the configuration of removed nodes that provides the minimal non-zero giant connected component.

A given node i can be disconnected from the giant component G , either because it is directly removed, or because it is indirectly detached by the removal of other nodes. In the former case $n_i = 0$, while in the second one $n_i = 1$. Thus, we see that n_i cannot tell us whether node i belongs to G or not. We then need another variable encoding the information that node i belongs or not to G . This variable is the probability of node i to belong to the giant connected component, ν_i , and we agree to set $\nu_i = 1$ if $i \in G$, and $\nu_i = 0$ otherwise. The fraction of nodes in the giant component, upon removing q of them from the network,

is then given by:

$$G(q) = \frac{1}{N} \sum_{i=1}^N \nu_i . \quad (8)$$

In principle, optimal percolation minimizes the giant component over the configurations \mathbf{n} . However an explicit functional form of $G(\mathbf{n})$ is not feasible. Our approach is to transform the problem into the minimization over \mathbf{n} of the largest eigenvalue controlling the stability of the percolation solution, which can be written explicitly in terms of \mathbf{n} . We first derive the relation between the vector $\boldsymbol{\nu} = (\nu_1, \dots, \nu_N)$ and the vector $\mathbf{n} = (n_1, \dots, n_N)$. This can be easily done using a message passing approach [22, 23, 36].

Let us consider two connected nodes i and j and orient the corresponding edge from i to j . Now let us suppose to "virtually" remove j (create a "cavity" at j) from the network and ask ourselves if node i belongs to G or not. This information can be stored in an auxiliary quantity $\nu_{i \rightarrow j} = 1, 0$ representing the probability of i to belong to the giant connected component in the absence of j . The advantage of using the variables $\nu_{i \rightarrow j}$, instead of ν_i is the fact that they satisfy a closed set of equations. Clearly $\nu_{i \rightarrow j} = 0$ if $n_i = 0$. So the interesting case is when $n_i = 1$. Recalling that j is momentarily absent from the network, the chance that i belongs to G is determined by the event "at least one among the neighbours of i different from j , belongs to G when i itself is virtually removed from the network". For a locally tree-like network this statement can be mathematically translated in the following message passing formula [22, 23]:

$$\nu_{i \rightarrow j} = n_i \left[1 - \prod_{k \in \partial i \setminus j} (1 - \nu_{k \rightarrow i}) \right] , \quad (9)$$

where $\partial i \setminus j$ is set of nearest neighbours of i minus j . We can finally put back j in the network and get the real information ν_i as:

$$\nu_i = n_i \left[1 - \prod_{k \in \partial i} (1 - \nu_{k \rightarrow i}) \right] . \quad (10)$$

The system defined by Eq. (9) always admits the solution $\{\nu_{i \rightarrow j} = 0\}$ for all $i \rightarrow j$ (regardless of the values of n_i), as can be verified by inspection.

As a consequence also $\{\nu_i = 0\}$ for all i , which in turn gives $G = 0$. This solution is stable, provided that the largest eigenvalue of the linear operator represented by the $2M \times 2M$ matrix defined on the directed links $k \rightarrow \ell, i \rightarrow j$:

$$\mathcal{M}_{k \rightarrow \ell, i \rightarrow j} = \left. \frac{\partial \nu_{i \rightarrow j}}{\partial \nu_{k \rightarrow \ell}} \right|_{\{\nu_{i \rightarrow j} = 0\}} \quad (11)$$

is less than one. We call $\lambda(\mathbf{n}; q)$ the largest eigenvalue of $\hat{\mathcal{M}}$, which depends on the vector \mathbf{n} and we add also a parametric dependence on the fraction of removed nodes q . Thus, the stability of a solution set \mathbf{n} of $G = 0$ is determined by the condition $\lambda(\mathbf{n}; q) < 1$.

For a fixed fraction q there exist, in general, very many possible configurations \mathbf{n} that satisfy Eq. (6). When $q < q_c$ each configuration \mathbf{n} gives $\lambda(\mathbf{n}; q) > 1$, since it is impossible to find a set of nodes to remove such that $G(q) = 0$, and this corresponds to the instability of the solution $\{\nu_{i \rightarrow j} = 0\}$ signaled by a value of $\lambda(\mathbf{n}; q)$ larger than one. On the contrary, when $q > q_c$, we have two different possibilities: there exist configurations \mathbf{n} such that $\lambda(\mathbf{n}; q) > 1$, which corresponds to nonoptimal node removals unable to destroy the giant component ($G(q) > 0$); on the other hand, there can be found other configurations for which $\lambda(\mathbf{n}; q) < 1$, which corresponds to a fragmented network with $G(q) = 0$. As we approach q_c from above, $q \rightarrow q_c^+$, the number of configurations \mathbf{n} such that $\lambda(\mathbf{n}; q) < 1$ (and hence $G(q) = 0$) decreases and eventually vanishes at q_c . This situation is exemplified in Fig. 1c.

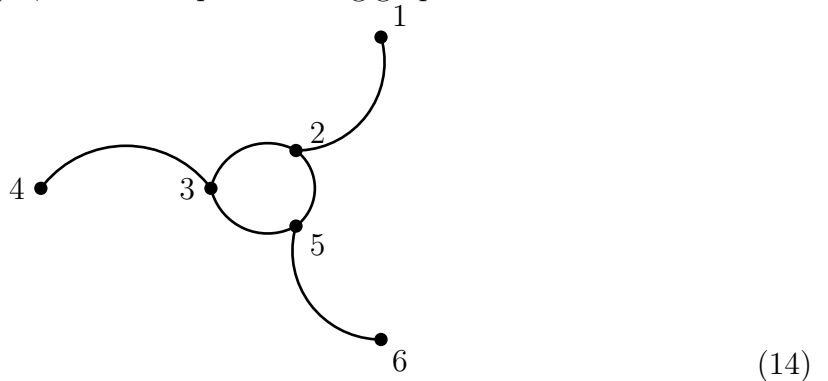
We find that the matrix $\hat{\mathcal{M}}$ is given in terms of the Non-Backtracking (NB) matrix $\hat{\mathcal{B}}$ [15, 24] for a locally-tree like random network via the equation:

$$\mathcal{M}_{k \rightarrow \ell, i \rightarrow j} = n_i \mathcal{B}_{k \rightarrow \ell, i \rightarrow j} \quad (12)$$

where

$$\mathcal{B}_{k \rightarrow \ell, i \rightarrow j} = \begin{cases} 1 & \text{if } \ell = i \text{ and } j \neq k, \\ 0 & \text{otherwise.} \end{cases} \quad (13)$$

The modified NB operator $\hat{\mathcal{M}}$ is represented by a $2M \times 2M$ matrix on the $2M$ directed edges of the network. For example, for the simple following graph with $N = 6$ and $M = 6$:



the corresponding $\hat{\mathcal{M}}$ matrix is a 12×12 matrix that reads (the associated non-backtracking matrix $\hat{\mathcal{B}}$ is obtained by setting $n_i = 1$):

$$\begin{array}{cccccccccccc}
 & 1 \rightarrow 2 & 2 \rightarrow 1 & 2 \rightarrow 3 & 2 \rightarrow 5 & 3 \rightarrow 2 & 3 \rightarrow 4 & 3 \rightarrow 5 & 4 \rightarrow 3 & 5 \rightarrow 2 & 5 \rightarrow 3 & 5 \rightarrow 6 & 6 \rightarrow 5 \\
 1 \rightarrow 2 & 0 & 0 & n_2 & n_2 & 0 & 0 & 0 & 0 & 0 & 0 & 0 & 0 \\
 2 \rightarrow 1 & 0 & 0 & 0 & 0 & 0 & 0 & 0 & 0 & 0 & 0 & 0 & 0 \\
 2 \rightarrow 3 & 0 & 0 & 0 & 0 & 0 & n_3 & n_3 & 0 & 0 & 0 & 0 & 0 \\
 2 \rightarrow 5 & 0 & 0 & 0 & 0 & 0 & 0 & 0 & 0 & 0 & n_5 & n_5 & 0 \\
 3 \rightarrow 2 & 0 & n_2 & 0 & n_2 & 0 & 0 & 0 & 0 & 0 & 0 & 0 & 0 \\
 3 \rightarrow 4 & 0 & 0 & 0 & 0 & 0 & 0 & 0 & 0 & 0 & 0 & 0 & 0 \\
 3 \rightarrow 5 & 0 & 0 & 0 & 0 & 0 & 0 & 0 & 0 & n_5 & 0 & n_5 & 0 \\
 4 \rightarrow 3 & 0 & 0 & 0 & 0 & n_3 & 0 & n_3 & 0 & 0 & 0 & 0 & 0 \\
 5 \rightarrow 2 & 0 & n_2 & n_2 & 0 & 0 & 0 & 0 & 0 & 0 & 0 & 0 & 0 \\
 5 \rightarrow 3 & 0 & 0 & 0 & 0 & n_3 & n_3 & 0 & 0 & 0 & 0 & 0 & 0 \\
 5 \rightarrow 6 & 0 & 0 & 0 & 0 & 0 & 0 & 0 & 0 & 0 & 0 & 0 & 0 \\
 6 \rightarrow 5 & 0 & 0 & 0 & 0 & 0 & 0 & 0 & 0 & n_5 & n_5 & 0 & 0
 \end{array} \tag{15}$$

The largest eigenvalue of the NB matrix $\hat{\mathcal{B}}$ is positive and simple, as a consequence of the Perron-Frobenius theorem [24], and the corresponding eigenvector is such that all components are positive.

The NB matrix $\hat{\mathcal{B}}$ has recently received a lot of attention in context of detectability of communities in complex networks [25, 26]. In that problem the interesting eigenvalue is the second largest, since the corresponding eigenvector can be used to label the nodes in different communities. This can be easily understood for the case of two communities. Since the eigenvector corresponding to the second largest eigenvalue has both positive and negative components, one can assign to one community all the nodes corresponding to the positive entries of the eigenvector, and to the other community all the nodes labeled with the negative components (the eigenvector corresponding to the largest eigenvalue does not work to define communities since it has all positive components, so that it is insensitive to the community structure of the network). This clustering method can be also generalized to the case of multiple (i.e. more than two) communities. This kind of community detection protocol can be implemented also using other matrices, e.g. the adjacency and the Laplacian matrices. What is crucial is the fact that the NB operator has the optimal performance, in

the sense that it is able to detect communities down to the detectability threshold, while the other spectral methods fail much before.

The NB matrix $\hat{\mathcal{B}}$ also intervenes when one linearizes the belief propagation equations, and it was first used to detect the location of the phase transition in Ref. [16] for the 3-coloring problem.

In our problem we are interested in the largest eigenvalue of the matrix $\hat{\mathcal{M}}$ (not of $\hat{\mathcal{B}}$), which is indeed a suitable modification of the NB matrix via optimal removal of n_i . That is, $\hat{\mathcal{M}}$ is a NB matrix on a modified network where some nodes are removed in an optimal way ($n_i = 0$). According to the Perron-Frobenius theorem, the largest eigenvalue of the matrix $\hat{\mathcal{B}}$ is a strictly decreasing function of $\hat{\mathcal{B}}$, that is if $\hat{\mathcal{M}} \leq \hat{\mathcal{B}}$ (meaning that the inequality holds entry by entry of the matrices) and $\hat{\mathcal{M}} \neq \hat{\mathcal{B}}$, then $\lambda(\hat{\mathcal{M}}) < \lambda(\hat{\mathcal{B}})$. In our case the matrix $\hat{\mathcal{M}}$ can be obtained from the matrix $\hat{\mathcal{B}}$ by setting one or some of the $n_i = 0$. Therefore the optimization problem for a given q can be rephrased as finding the optimal influencer configuration \mathbf{n}^* that minimize $\lambda(\mathbf{n}; q)$ over all possible configurations \mathbf{n} satisfying $\langle n \rangle = 1 - q$. Calling $\lambda(\mathbf{n}^*; q)$ this minimum, we write:

$$\lambda(\mathbf{n}^*; q) \equiv \min_{\mathbf{n}: \langle n \rangle = 1 - q} \lambda(\mathbf{n}; q) . \quad (16)$$

The optimal threshold q_c is the solution of the equation:

$$\lambda(\mathbf{n}^*; q_c) = 1. \quad (17)$$

Still, this equation is hard to solve, since there is no explicit formula for $\lambda(\mathbf{n}; q)$ as a function of \mathbf{n} . To tackle this problem we propose a sequence of approximations to the largest eigenvalue (and associated eigenvector) which is based on the Power Method iterative scheme that we find quickly convergent to the exact solution of the problem. We stress that the optimal exact solution for $\ell \rightarrow \infty$ holds only under the assumption that the graph under consideration is locally-tree like.

Before to conclude this section, we notice that for the network depicted in (14), the modified NB matrix does not depend on n_1, n_4, n_6 , i.e., it does not depend on the variables outside the loop. As a consequence, its largest eigenvalue does not depend on those variables as well: $\lambda = \lambda(n_2, n_3, n_5)$. Therefore, removing the nodes at the end of the dangling edge does not reduce the eigenvalue λ , which is one for the considered network: $\lambda(1, 1, 1) = 1$. On the contrary, by removing a node belonging to the loop, e.g. nodes 2, 3 or 5, the network

becomes a tree, and the eigenvalue is zero: $\lambda(0, 1, 1) = \lambda(1, 0, 1) = \lambda(1, 1, 0) = 0$. In general, the largest eigenvalue of a tree-network is equal to zero. For networks with one loop (unicyclic graph), the largest eigenvalue is equal to one, and for networks with many loops λ is larger than 1. Thus we see that the result of minimizing the largest eigenvalue of the modified NB matrix is a way to attack the loops in the network. When the eigenvalue reaches the critical value one ($\lambda = 1$) the network consists of a single loop, that is suddenly destroyed by the removal of a single node, causing the sharp drop of the eigenvalue from one to zero. When the giant component is reduced to a tree-like topology, it can be considered as completely fragmented, since any tree can be destroyed with a subextensive number of node removals. Thus, our theory suggests that the best attack strategy is to destroy the loops. This process is illustrated in Fig. 1c.

B. Mapping of optimal immunization and spreading problems onto optimal percolation

Here we map exactly the problems of optimal immunization and spreading to the problem of minimizing the giant component of a network, ie, optimal percolation.

In the immunization case, the quantity ν_i represents the probability of node i to be infected. Therefore minimizing the sum $\sum_i \nu_i$ is equivalent to minimize the size of the disease outbreak, which is obtained by optimally choosing the immunizator nodes. These immunizators are exactly the nodes we need to remove to fragment the network. Precisely, $n_i = 0$ if node i is an optimal immunizator, and $n_i = 1$ if not. Note that we can also slightly modify the equations to include the case of a transmission probability of the disease w smaller than one (the case treated explicitly in our paper corresponds to $w = 1$). Including w , the main equation reads:

$$\nu_{i \rightarrow j} = n_i \left[1 - \prod_{k \in \partial i \setminus j} (1 - w\nu_{k \rightarrow i}) \right]. \quad (18)$$

In this case the optimal immunizators can be still identified by minimizing the largest eigenvalue of the modified NB operator $\hat{\mathcal{M}}$. The only difference is that the critical threshold q_c is defined by the following equation:

$$\lambda(\mathbf{n}^*; q_c) = 1/w. \quad (19)$$

It should be noted, though, that the quantity $N^{-1} \sum_i \nu_i$, which quantifies the total fraction of infected individuals, is different from the giant component G when $w < 1$.

The case of optimal spreaders is the dual of the optimal immunizers. The optimized spreading problem [4] consists of finding the minimum number of nodes to "activate" in such a way that the information percolates the network following, for instance, the Linear Threshold Model (LTM) dynamics [17, 18]. The LTM simulates a spreading of information process where an individual adopts an opinion or information under "peer pressure", that is, it becomes activated only after a given number of its neighbors are [17, 18, 37, 38]. The optimal influence threshold represents the minimum fraction of spreader nodes we need to activate to spread the information all over the network. The mathematical formulation of the problem is the following. Let us define $\nu_{i \rightarrow j}$ as the probability that, in the information spreading process, node i is eventually NOT activated in absence of node j . Moreover, we assign to each node the number n_i , which, in this case, equals zero, $n_i = 0$, if i is an initial spreader, and $n_i = 1$ if not. We note that in the case of immunization, $n_i = 0$ corresponds to an immunized node. Following the Linear Threshold Model (LTM) [17] of information spreading, in order for node i to be activated in absence of node j , the neighbouring nodes such that $k \in \partial i \setminus j$ must be activated. In the Linear Threshold Model [17, 18], this situation corresponds to considering uniform weights $w_{ij} = 1$ for each edge (i, j) , and threshold of activation $\theta_i = k_i - 1$ for each node with degree k_i , such that a node i becomes activated if the number of active neighbors is at least θ_i . The optimal spreading problem under the LTM is to find the minimum set of initially activated spreaders, q_c , which will percolate the information to the entire network, as defined in Kempe *et al.* [4]. On the other limit, the optimal immunizer problem corresponds to setting $\theta_i = 1$, further showing the dual relation between the immunization and spreading problem.

The probabilities $\nu_{i \rightarrow j}$ for spreading can be computed self-consistently through the following message passing equations [22, 23, 36] in analogy to Eq. (9):

$$\nu_{i \rightarrow j} = n_i \left[1 - \prod_{k \in \partial i \setminus j} (1 - \nu_{k \rightarrow i}) \right]. \quad (20)$$

The total probability ν_i that i is not activated is obtained from Eq. (20) by including the contribution of $\nu_{j \rightarrow i}$ as well:

$$\nu_i = n_i \left[1 - \prod_{k \in \partial i} (1 - \nu_{k \rightarrow i}) \right], \quad (21)$$

and the total fraction of nodes not activated in the spreading process is:

$$G = \frac{1}{N} \sum_{i=1}^N \nu_i. \quad (22)$$

The optimization problem in spreading under the LTM consists in minimizing the fraction of inactive nodes G , or equivalently, maximizing the spreading over the network. We notice the dual nature of G in immunization and spreading. In the former, G represents the fraction of inactive nodes, which we want to minimize to maximize spreading. In the later, G represents the connected component of individuals who would get infected if the epidemic starts in a single node. In this case, we also want to minimize G to reduce the spread of the epidemic. This is the basic reason why we are able to bring the two problems under the same framework of optimal percolation.

In activated spreading, the minimization of G is achieved by optimally placing the initial spreaders $n_i = 0$. Equations (20) and (21) are formally identical to the equations of optimal influence (9), (10). To summarize, in spreading, the giant component G represents the fraction of inactivated nodes. Therefore, by minimizing the giant component in spreading we are effectively maximizing the spreading of information. This completes the mapping between the immunization and spreading problem to optimal percolation.

We notice that the mapping of the optimal LTM problem to optimal percolation is done for a threshold $\theta_i = k_i - 1$. For $\theta_i = 1$, we recover the optimal immunization problem. These two problems can be solved by studying the local stability of the solution $G = 0$ in both cases. This is possible since at q_c the transition is of second order, and thus a local stability theory is applicable. For other intermediate values of the threshold $\theta_i = k_i - 2, k_i - 3, \dots, 2$, the transition at q_c is of first order, of the type of bootstrap percolation [39]. In these regimes, a local stability criterion cannot be applied, and the optimal spreading problem in these cases needs to be considered independently. That is, the largest eigenvalue of the NB operator is not guaranteed to provide the optimal set when the transition is of first order. Nevertheless, we could expect that the proposed CI algorithm may work as well in this regime of discontinuous transition. Another interesting generalization of the present study is the case of randomly chosen heterogeneous threshold θ_i in the LTM [18] or a fix threshold

[38].

A further interesting optimization problem is to find the optimal spreaders under the SIR or SIS models [12]. In general, this problem cannot be translated into an optimal percolation problem, because it does not have a transition from $G = 0$ to $G > 0$. Therefore, it cannot be treated under our stability theory. However, as for the LTM with intermediate values of the threshold, the spreaders identified by the CI algorithm could still be expected to be close to optimal.

To conclude this section, we notice that for all optimization problems on locally tree-like random networks that can be mapped onto an optimal percolation problem, with a second order transition separating the phases with $G = 0$ and $G > 0$, our theory holds true, and the CI algorithm can be used accordingly.

In the next sections, we show that the optimal percolation set is obtained as a (infinite) sequence of optimized “attacks” expressed as successive approximations to the minimization of the largest eigenvalue of the modified non-backtracking matrix. At the most trivial level, we obtain the random attack of the network corresponding to random percolation, Eq. S28. The zero-order naive strategy corresponding to the lowest approximation of the theory is given by the attack on the high degree nodes, Eq. S70. The first non-trivial collective attack strategy is equivalent to find the ground state of a two-body spin-glass like system, i.e., an anti-ferromagnetic Ising model with random bonds in a random external field at fixed magnetization, Eq. S78. Higher-order approximations consist of increasing many-body problems, Eq. S53, and produce increasingly better performance compared to previous heuristic strategies.

C. Limit of applicability of the theory of influence

The mapping of the optimal influence problem onto the optimal percolation problem developed so far is strictly valid for locally tree-like networks: in the message passing formulation Eq. (9), the probabilities $\nu_{k \rightarrow i}$ are assumed to be independent. This includes the thermodynamic limit of the class of random networks of Erdős-Rényi, scale-free networks [5] and the configuration model (the maximally random graphs with a given distribution [40]) which are locally tree-like and contains loops that grow as $\log N$ [41]. Nonetheless, it is generally accepted, and confirmed by many works, that results obtained for tree-like graphs

apply quite well also for loopy networks, provided the density of loops is not excessively large [14, 25, 36]. Wherever the number of such topological structures (loops) is abundant (e.g., to finite dimensional lattices), the quality of the results obtained for tree-like networks deteriorates. Indeed, the locally tree-like approximation has been successfully used for a plethora of other problems, like spin glass models on random graphs, coloring, matching, bisection and maximum cut of graphs, and many other constraint satisfaction problems [36].

D. Random influence

The trivial case corresponds to random removal of nodes (random percolation). It is obtained by taking the n_i at random from the distribution $P(\mathbf{n}; q)$ such that the removal is decoupled from the non-backtracking matrix:

$$P(\mathbf{n}; q) = \prod_{i=1}^N (1 - q)^{n_i} q^{1 - n_i} . \quad (23)$$

Taking the expectation of the matrix \mathcal{M} over \mathbf{n} , and exploiting the fact that $P(\mathbf{n}; q)$ is factorized over the sites, Eq. (12) becomes:

$$\mathbb{E}_{\mathbf{n}} \mathcal{M}_{i \rightarrow j, k \rightarrow \ell} = (1 - q) \mathcal{B}_{i \rightarrow j, k \rightarrow \ell} . \quad (24)$$

Therefore, the eigenvalue $\lambda(\mathbf{n}; q)$, averaged over \mathbf{n} , is given by:

$$\lambda(q) = (1 - q) \lambda_{\hat{\mathcal{B}}} , \quad (25)$$

where $\lambda_{\hat{\mathcal{B}}}$ is the largest eigenvalue of the NB matrix $\hat{\mathcal{B}}$ for a random network. It is well known that the largest eigenvalue of the NB matrix is equal to [25]:

$$\lambda_{\hat{\mathcal{B}}} = \kappa - 1 , \quad (26)$$

with κ equals to the ratio of the first two moments of the degree distribution:

$$\kappa = \langle k^2 \rangle / \langle k \rangle . \quad (27)$$

The condition $\lambda(q_c) = 1$ is nothing but the famous result for random percolation [21] which has been obtained using the NB matrix in [23, 27], i.e.:

$$q_c^{\text{ran}} = 1 - (\kappa - 1)^{-1} . \quad (28)$$

Thus, when \mathbf{n} is decoupled with the NB matrix, the largest eigenvalue of NB captures the random percolation threshold for random networks. This result has been previously obtained in [23] using similar ideas as used in the present derivation. The largest eigenvalue of the NB matrix in case of random removal of nodes is true only when the original graph is random. For a generic graph, the largest eigenvalue can be very different and not related to the first and second moment of the degree distribution. On the other hand, the optimal threshold arises by coupling the removal of nodes with the NB matrix, a case that is treated next.

E. Derivation of the main formula: cost energy function of influence, Eq. (4)

Next, we derive Eq. (4) which holds only on very large locally tree-like graphs. From now on we omit q in $\lambda(\mathbf{n}; q) \equiv \lambda(\mathbf{n})$, which is always kept fixed. For a given configuration \mathbf{n} , the eigenvalue $\lambda(\mathbf{n})$ determines the growth rate of an arbitrary nonzero vector \mathbf{w}_0 after ℓ iterations of the matrix $\hat{\mathcal{M}}$, provided that \mathbf{w}_0 has nonzero projection onto the eigenvector corresponding to $\lambda(\mathbf{n})$. Denoting with $\mathbf{w}_\ell(\mathbf{n})$ the vector at the ℓ -th iteration,

$$\mathbf{w}_\ell(\mathbf{n}) = \hat{\mathcal{M}}^\ell \mathbf{w}_0, \quad (29)$$

we can write according to Power Method [42]:

$$\lambda(\mathbf{n}) = \lim_{\ell \rightarrow \infty} \left[\frac{|\mathbf{w}_\ell(\mathbf{n})|}{|\mathbf{w}_0|} \right]^{1/\ell}, \quad (30)$$

where

$$|\mathbf{w}_\ell(\mathbf{n})|^2 = \langle \mathbf{w}_\ell(\mathbf{n}) | \mathbf{w}_\ell(\mathbf{n}) \rangle = \langle \mathbf{w}_0 | (\hat{\mathcal{M}}^\ell)^\dagger \hat{\mathcal{M}}^\ell | \mathbf{w}_0 \rangle. \quad (31)$$

For finite ℓ we define the ℓ -dependent approximant $\lambda_\ell(\mathbf{n})$ as:

$$\lambda_\ell(\mathbf{n}) = \left[\frac{|\mathbf{w}_\ell(\mathbf{n})|}{|\mathbf{w}_0|} \right]^{1/\ell}, \quad (32)$$

so that we have:

$$\lambda(\mathbf{n}) = \lim_{\ell \rightarrow \infty} \lambda_\ell(\mathbf{n}). \quad (33)$$

We now derive the analytical expression of $\lambda_\ell(\mathbf{n})$.

We start by computing the first approximant $\ell = 1$:

$$|\mathbf{w}_1(\mathbf{n})\rangle = \hat{\mathcal{M}}|\mathbf{w}_0\rangle. \quad (34)$$

In order to do this, it is convenient to embed the matrix $\hat{\mathcal{M}}$, whose dimension is $2M \times 2M$, in a larger space of dimension $N \times N \times N \times N$. In this enlarged space $\hat{\mathcal{M}}$ is given by:

$$\mathcal{M}_{ijkl} = n_k A_{ij} A_{kl} \delta_{jk} (1 - \delta_{il}) , \quad (35)$$

where each index runs from 1 to N : $i, j, k, \ell = 1, \dots, N$, and A_{ij} is the adjacency matrix. Practically, we have represented $\hat{\mathcal{M}}$ on the nodes of the network, rather than on the directed edges. The Kronecker deltas guarantee the non-backtracking nature of the NB walks.

As starting $2M$ -dimensional vector $|\mathbf{w}_0\rangle = |\mathbf{1}\rangle$ in the space of links, we choose the vector with all components equal one; the optimal solution is independent of this selection. The components of the analogous $N \times N$ vector, $|\mathbf{w}_0\rangle$ in the enlarged space of nodes are given by $|w_0\rangle_{ij} = A_{ij}$.

The right vector $|\mathbf{w}_1(\mathbf{n})\rangle$ is computed as:

$$|w_1(\mathbf{n})\rangle_{ij} = \sum_{k\ell} \mathcal{M}_{ijkl} |w_0\rangle_{k\ell} = n_j A_{ij} (k_j - 1) , \quad (36)$$

while the left vector $\langle \mathbf{w}_1(\mathbf{n})|$ is given by:

$${}_{ij}\langle w_1(\mathbf{n})| = \sum_{k\ell} {}_{k\ell}\langle w_0| \mathcal{M}_{k\ell ij} = n_i A_{ij} (k_i - 1) . \quad (37)$$

The factor $k_i - 1$ will appear frequently in the following, so it is worth to set the residual degree:

$$z_i \equiv k_i - 1 . \quad (38)$$

The norm $|\mathbf{w}_1(\mathbf{n})|^2$ is:

$$|\mathbf{w}_1(\mathbf{n})|^2 = \sum_{ij} {}_{ij}\langle w_1(\mathbf{n})| w_1(\mathbf{n}) \rangle_{ij} = \sum_{ij} A_{ij} z_i z_j n_i n_j . \quad (39)$$

Since the norm of $|\mathbf{w}_0\rangle$ is simply: $|\mathbf{w}_0|^2 = \sum_i k_i = 2M$, we can write the final expression for $\lambda_1(\mathbf{n})$ from Eq. (32) as:

$$\lambda_1(\mathbf{n}) = \left[\frac{1}{2M} \sum_{ij} A_{ij} z_i z_j n_i n_j \right]^{1/2} . \quad (40)$$

It is useful to give a graphical representation of the previous formula in terms of a diagrammatic expansion, which becomes indispensable for higher orders of the iteration. The

interaction term in the sum in the numerator on the r.h.s of Eq. (40) can be represented as

$$A_{ij}(k_i - 1)(k_j - 1)n_i n_j = \begin{array}{c} z_i \\ \text{wavy line} \\ n_i \end{array} \begin{array}{c} \longrightarrow \\ \text{straight line} \\ \longrightarrow \end{array} \begin{array}{c} z_j \\ \text{wavy line} \\ n_j \end{array} \quad (41)$$

The meaning of the diagram is the following: each time a straight line connects two sites i and j , the variables n_i and n_j are multiplied by each other (the meaning of the arrow is explained later in Methods Section IIF in terms of NB walks; for the moment it can be thought of as an undirected line). The wiggly lines on the nodes means a multiplication by the factor $z_i = k_i - 1$. The diagram is then equal to $n_i n_j z_i z_j$. The number of variables appearing in the diagram gives the order of the interaction. In this case, corresponds to a pair-wise interaction. Thus, the first optimization order $\ell = 1$ corresponds to a 2-body problem. We will see that, in general, the ℓ -order term in the approximant describes a 2ℓ -body problem.

Let us compute for $\ell = 2$, $|\mathbf{w}_2(\mathbf{n})\rangle$:

$$|w_2(\mathbf{n})\rangle_{ij} = \sum_{k\ell} \mathcal{M}_{ijk\ell} |w_1(\mathbf{n})\rangle_{k\ell} = n_j A_{ij} \sum_{\ell} A_{j\ell} n_{\ell} z_{\ell} (1 - \delta_{i\ell}), \quad (42)$$

and also $\langle \mathbf{w}_2(\mathbf{n})|$:

$${}_{ij} \langle w_2(\mathbf{n})| = \sum_{k\ell} {}_{k\ell} \langle w_1(\mathbf{n})| \mathcal{M}_{k\ell ij} = n_i A_{ij} \sum_k A_{ik} n_k z_k (1 - \delta_{kj}). \quad (43)$$

The norm $|\mathbf{w}_2(\mathbf{n})|^2$ is given by:

$$|\mathbf{w}_2(\mathbf{n})|^2 = \sum_{ijkl} A_{ij} A_{jk} A_{k\ell} (1 - \delta_{ik}) (1 - \delta_{j\ell}) z_i z_{\ell} n_i n_j n_k n_{\ell}. \quad (44)$$

There are two types of interactions in the sum on the r.h.s of Eq. (44): a 4-body and a 3-body interaction. The graphical representation of the former is:

$$A_{ij} A_{jk} A_{k\ell} z_i z_{\ell} n_i n_j n_k n_{\ell} = \begin{array}{c} z_i \\ \text{wavy line} \\ n_i \end{array} \begin{array}{c} \longrightarrow \\ \text{straight line} \\ \longrightarrow \end{array} \begin{array}{c} n_j \\ \longrightarrow \\ \text{straight line} \\ \longrightarrow \end{array} \begin{array}{c} n_k \\ \longrightarrow \\ \text{straight line} \\ \longrightarrow \end{array} \begin{array}{c} z_{\ell} \\ \text{wavy line} \\ n_{\ell} \end{array} \quad (45)$$

The diagram for the 3-body interaction is:

$$A_{ij} A_{jk} A_{ki} (z_i)^2 n_i n_j n_k = \begin{array}{c} n_i \\ \text{wavy line} \\ \text{triangle} \\ \text{wavy line} \\ z_i \end{array} \begin{array}{c} \longrightarrow \\ \text{straight line} \\ \longrightarrow \end{array} \begin{array}{c} z_i \\ \text{wavy line} \\ n_j \end{array} \begin{array}{c} \longrightarrow \\ \text{straight line} \\ \longrightarrow \end{array} \begin{array}{c} z_i \\ \text{wavy line} \\ n_k \end{array} \quad (46)$$

F. Interpretation in terms of NB walks and generalization to 2ℓ -body interactions

Nodes entering in each type of interaction given by $|\mathbf{w}_1(\mathbf{n})|^2$, $|\mathbf{w}_2(\mathbf{n})|^2$, and $|\mathbf{w}_3(\mathbf{n})|^2$ are the same nodes visited by a non-backtracking walk of length 1, 3, 5, respectively (with the possibility of traversing an edge multiple times). In general, the diagrammatic expansion of the term $|\mathbf{w}_\ell(\mathbf{n})|^2$ will then contain all the possible graphs that can be built using the nodes traversed by a NB-walk of length $2\ell - 1$. This is the reason why we put an arrow in the diagrammatic schematization of the interaction terms: emphasizing the connection with NB walks.

The NB graphs in the expansion are built in the following way: (a) For a given ℓ we construct all NB walks of $2\ell - 1$ steps starting at one node i (with degree k_i) and ending in node j (with degree k_j). The initial and ending point are indicated by a wiggly line indicating their degree minus one. (b) The initial and final node of the NB walk do not need to be necessarily different. (c) Loops are allowed in the NB walk. Thus, the shortest path between i and j might be smaller than the $2\ell - 1$ steps of the walk. (d) We recall that the condition for a NB random walk is only that it cannot come back through the same link that it just came on, yet, it can visit the same node several times. (e) As well, the NB walks are allowed to travel through the same links multiple times. (f) The number of nodes of the NB walk is the order of the interaction. (g) The dominant graph is always a direct path (line) of length $2\ell - 1$ and 2ℓ nodes, where the shortest path between the initial and ending node is $2\ell - 1$; we will see that all the other diagrams with loops are negligible for sparse locally tree-like random graphs.

For instance, in the case $\ell = 2$, we obtain two graphs representing NB walks of length $2\ell - 1 = 3$. The graph (45) represents a NB walk of length 3 which traverses 4 distinct nodes, and thus it is a 4-body dominant interaction. The graph (46) also represents a NB walk of length 3, but this time the NB walk starts and ends in the same node i , rule (b) and (c), so this term contributes with a factor z_i^2 .

In the case $\ell = 3$, the leading interaction is graph (49) of 6-body interactions and 5 NB steps. The 3-body interaction (49) is a NB walk of 5 steps that starts at the node i on the right and traverses two links twice, rule (e), to end up in node j , resulting in a triangular 3-body problem.

Next, we show that, in a sparse random network, all the NB graphs with loops can be

neglected to $O(1/N)$, in accordance with the assumption of locally-tree like structure. Thus, the main equation (4) takes into account only the leading 2ℓ -body interaction for each ℓ -level in the diagrammatic expansion to $O(1/N)$. This situation is translated to the CI algorithm where the ball is defined by a radius ℓ defined as the shortest path between two nodes in the network.

It is important to note that, for locally tree-like graphs and for very large system sizes N , the terms containing one or more loops are suppressed by powers of $1/N$. This can be understood through the following argument. Let us consider, for the sake of simplicity, an ER random graph, where each edge is present with probability z/N , where z is the average degree (in ER the average degree is the same as the average residual degree). The total number of loops in ER of given length ℓ is given on average by (the final formula is valid for general sparse random graphs [40], the quantity z being in general the average residual degree):

$$\mathcal{N}(\ell) = \left(\frac{z}{N}\right)^\ell \frac{1}{2\ell} N(N-1)\dots(N-\ell+1) \sim \frac{z^\ell}{2\ell}, \quad (50)$$

where the factor $1/2\ell$ comes from the fact that: i) anyone of the ℓ nodes in the loop can be taken as starting point; ii) the loop can be traveled in two directions. Therefore, the probability $p(\ell)$ for a node to belong to a loop of length ℓ is:

$$p(\ell) = \frac{\mathcal{N}(\ell)}{N} = \frac{z^\ell}{2\ell N}, \quad (51)$$

and thus it is of order $O(1/N)$. The quantity $\mathcal{N}(\ell)$ enumerates the number of non self-intersecting closed walks. Self-intersecting closed walks have a probability of order $O(1/N^2)$, since the self-intersection is encountered, on average, in a fraction $1/N^2$ of the total number of nodes. Thus, loops with many self-intersections are suppressed by higher power of $1/N$. This argument can be generalized to random graph ensembles other than ER, provided they have a locally tree-like structure in the limit $N \rightarrow \infty$.

As a consequence, for very large network, the leading term of $|\mathbf{w}_\ell(\mathbf{n})|^2$ for a given ℓ (i.e., the one containing a number of nodes exactly equal to 2ℓ , for instance the diagram (48) in the expression of $|\mathbf{w}_3(\mathbf{n})|^2$) is already a good approximation, which becomes exact for $N \rightarrow \infty$. However, for small networks all the terms should be considered. In Methods Section IV, we will minimize the eigenvalue $\lambda_\ell(\mathbf{n})$ by taking into account all the possible interactions.

Since, in the limit $N \rightarrow \infty$, loops do not contribute to the assessment of the norm $|\mathbf{w}_\ell(\mathbf{n})|$, the equation for $|\mathbf{w}_\ell(\mathbf{n})|$ simplifies considerably, because we can take into account only the terms with exactly 2ℓ -body interactions; the remaining ones with loops decay as $1/N$ or faster.

The analytical expression for $|\mathbf{w}_1(\mathbf{n})|^2$ and $|\mathbf{w}_2(\mathbf{n})|^2$ given by Eqs. (39), (44) can be generalized to any $|\mathbf{w}_\ell(\mathbf{n})|^2$. We get

$$|\mathbf{w}_\ell(\mathbf{n})|^2 = \sum_{i_1 i_2 \dots i_{2\ell}} A_{i_1 i_2} A_{i_2 i_3} \dots A_{i_{2\ell-1} i_{2\ell}} (1 - \delta_{i_1 i_3}) (1 - \delta_{i_2 i_4}) \dots (1 - \delta_{i_{2\ell-2} i_{2\ell}}) z_{i_1} z_{i_{2\ell}} n_{i_1} n_{i_2} \dots n_{i_{2\ell}}. \quad (52)$$

Each term of the sum in Eq. (52) can be associated to a non backtracking walk of length $2\ell - 1$, where edges may be crossed multiple times. To each node visited by the NB walk is attached a variable n_i , and the extreme nodes of the walk have the extra factors z_{i_1} (starting point) and $z_{i_{2\ell}}$ (end point). When NB walks containing loops are neglected in Eq. (52), the formula simplifies considerably, since the only remaining walks are the ones of length $2\ell - 1$ where each one of the 2ℓ nodes is visited only once. For example, let us consider a loop free NB walk of length $2\ell - 1$ starting from a given node, say node i . It visits all nodes up to a distance $2\ell - 1$, and stops at the final node, say node j . The total number of nodes visited by this NB walk is 2ℓ .

Notice that, when loops are neglected, we can approximate the local environment around any node by a tree, in line with the original locally-tree like assumption of the whole approach. A simple way to implement the tree-like approximation is to consider only the NB walks of length $2\ell - 1$ that start from a given node i and end on nodes j , in such a way that these NB walks coincide with the shortest paths between i and those nodes j . Moreover, these NB walks contain the products $n_{i_1} n_{i_2} \dots n_{i_{2\ell}}$ with all n_{i_α} different from each other. Hence, we can finally write down the expression for the leading term of $|\mathbf{w}_\ell(\mathbf{n})|^2$ as:

$$|\mathbf{w}_\ell(\mathbf{n})|^2 = \sum_{i=1}^N z_i \sum_{j \in \partial \text{Ball}(i, 2\ell-1)} \left(\prod_{k \in \mathcal{P}_{2\ell-1}(i,j)} n_k \right) z_j, \quad (53)$$

where $\text{Ball}(i, \ell)$ is the set of nodes inside a ball of radius ℓ around node i , where the radius is defined taking the shortest path as the distance, $\partial \text{Ball}(i, \ell)$ is the frontier of the ball and $\mathcal{P}_\ell(i, j)$ is the set of nodes belonging to the shortest path of length ℓ connecting i and j . This is the cost energy function of influence Eq. (4) given in the main text.

G. Odd $(2\ell + 1)$ -body interactions

The energy (or cost) function Eq. (53) contains only even 2ℓ -body interactions. It is possible to interpolate with odd interactions by considering an analogous Power Method expansion of the eigenvalue in terms of the matrix elements $\langle \mathbf{w}_\ell(\mathbf{n}) | \hat{\mathcal{M}} | \mathbf{w}_\ell(\mathbf{n}) \rangle$. Indeed, the eigenvalue $\lambda(\mathbf{n})$ can be also computed using another series expansion in the Power Method [42] as:

$$\lambda(\mathbf{n}) = \lim_{\ell \rightarrow \infty} \left[\frac{\langle \mathbf{w}_\ell(\mathbf{n}) | \hat{\mathcal{M}} | \mathbf{w}_\ell(\mathbf{n}) \rangle}{\langle \mathbf{w}_0 | \mathbf{w}_0 \rangle} \right]^{1/(2\ell+1)}. \quad (54)$$

The explicit expression of $\langle \mathbf{w}_\ell(\mathbf{n}) | \hat{\mathcal{M}} | \mathbf{w}_\ell(\mathbf{n}) \rangle$ can be computed similarly to $|\mathbf{w}_\ell(\mathbf{n})|^2$, following the same steps outlined in Methods Section II E. As an example, for $\langle \mathbf{w}_1(\mathbf{n}) | \hat{\mathcal{M}} | \mathbf{w}_1(\mathbf{n}) \rangle$ we get:

$$\langle \mathbf{w}_1(\mathbf{n}) | \hat{\mathcal{M}} | \mathbf{w}_1(\mathbf{n}) \rangle = \sum_{ijk} A_{ij} A_{jk} (1 - \delta_{ik}) z_i z_k n_i n_j n_k. \quad (55)$$

The asymptotic expression for $N \rightarrow \infty$ (i.e. the one neglecting loops) is similar to Eq. (53), and, for $\ell \geq 1$, reads:

$$\langle \mathbf{w}_\ell(\mathbf{n}) | \hat{\mathcal{M}} | \mathbf{w}_\ell(\mathbf{n}) \rangle = \sum_{i=1}^N z_i \sum_{j \in \partial \text{Ball}(i, 2\ell)} \left(\prod_{k \in \mathcal{P}_{2\ell}(i, j)} n_k \right) z_j, \quad (56)$$

while for $\ell = 0$ we find:

$$\langle \mathbf{w}_0 | \hat{\mathcal{M}} | \mathbf{w}_0 \rangle = \sum_{i=1}^N k_i (k_i - 1) n_i. \quad (57)$$

We can introduce the equivalent of the approximant $\lambda_\ell(\mathbf{n})$ in Eq. (32), that we call $\lambda'_\ell(\mathbf{n})$:

$$\lambda'_\ell(\mathbf{n}) = \left[\frac{\langle \mathbf{w}_\ell(\mathbf{n}) | \hat{\mathcal{M}} | \mathbf{w}_\ell(\mathbf{n}) \rangle}{\langle \mathbf{w}_0 | \mathbf{w}_0 \rangle} \right]^{1/(2\ell+1)}. \quad (58)$$

H. HD attack at $\ell = 0$ one-body problem

It is interesting to consider the $\ell = 0$ term, $\lambda'_0(\mathbf{n})$, since it reproduces exactly the high-degree (HD) strategy attacking the hubs calculated by Cohen *et al.* [10]. This term represents the one-body interaction where the influencers are considered in isolation, only affected by the external field, and therefore this strategy lacks the collective influence effects found

for $\ell \geq 2$. It reads:

$$\lambda'_0(\mathbf{n}) = \frac{\langle \mathbf{w}_0 | \hat{\mathcal{M}} | \mathbf{w}_0 \rangle}{\langle \mathbf{w}_0 | \mathbf{w}_0 \rangle} = \frac{\sum_i k_i(k_i - 1)n_i}{\sum_i k_i} . \quad (59)$$

The sum on the numerator on the r.h.s represents the energy of a gas of free particles in an external (site-dependent) field $h_i = k_i(k_i - 1)$. This field is always nonnegative $h_i \geq 0$. Therefore, in order to minimize $\lambda'_0(\mathbf{n})$ it is sufficient to sort the nodes according to the external field, and then removing the ones corresponding to the highest Nq fields. Since the field h_i is monotonic increasing with the degree, the minimization corresponds exactly to the removal of the high degree nodes one by one. It is also easy to see that the stability condition imposed on $\lambda'_0(\mathbf{n})$,

$$\min_{\mathbf{n}: \langle n \rangle = 1 - q_c} \lambda'_0(\mathbf{n}) = 1, \quad (60)$$

gives exactly the threshold q_c expected from HD as calculated by Cohen *et al.* [10]. Indeed, putting the expression for $\lambda'_0(\mathbf{n})$ in Eq. (60), we have,

$$\min_{\mathbf{n}: \langle n \rangle = 1 - q_c} \frac{\sum_i k_i(k_i - 1)n_i}{\sum_i k_i} = 1 . \quad (61)$$

As we said, the minimization of the numerator in the l.h.s. is achieved by setting $n_i = 0$ for the first Nq_c highest degree node, and $n_i = 1$ for the remaining ones. Therefore we can rewrite Eq. (61) as:

$$\frac{1 - q_c}{\langle k \rangle} (\langle k^2 \rangle' - \langle k \rangle') = 1 , \quad (62)$$

where the average $\langle \cdot \rangle'$ is performed using a modified degree distribution $P'(k; q_c)$, which depends on q_c and represents the degree distribution in the network with the removed hubs. To derive the explicit form of $P'(k; q_c)$, let us consider first the relation between q_c and the original $P(k)$. The fraction q_c of nodes to be removed is

$$\sum_{k=\zeta}^{\infty} P(k) = q_c , \quad (63)$$

where ζ is the lowest degree of the removed nodes compatible with q_c .

The distribution $P'(k; q_c)$ is the degree distribution of the remaining nodes (i.e. the ones for which $n_i = 1$) and is given by:

$$P'(k; q_c) = \frac{1}{1 - q_c} P(k) \theta(\zeta - k) . \quad (64)$$

We now solve Eq. (61) in the case of scale free network with degree distribution $P(k) \sim k^{-\gamma}$, degree exponent γ , minimum degree m and maximum degree k_{\max} . We also work in

the continuum limit, so that we can use integrals in place of the sums. The variable ζ as a function of q_c reads:

$$q_c = \int_{\zeta}^{k_{\max}} P(k) k dk = \frac{\zeta^{1-\gamma} - k_{\max}^{1-\gamma}}{m^{1-\gamma} - k_{\max}^{1-\gamma}}. \quad (65)$$

The average $\langle k \rangle'$ is given by:

$$\langle k \rangle' = \frac{1}{1 - q_c} \int_m^{\zeta} P(k) k dk = \frac{1}{1 - q_c} \frac{\gamma - 1}{\gamma - 2} \frac{m^{2-\gamma} - \zeta^{2-\gamma}}{m^{1-\gamma} - k_{\max}^{1-\gamma}}, \quad (66)$$

and $\langle k^2 \rangle'$ by:

$$\langle k^2 \rangle' = \frac{1}{1 - q_c} \frac{\gamma - 1}{\gamma - 3} \frac{m^{3-\gamma} - \zeta^{3-\gamma}}{m^{1-\gamma} - k_{\max}^{1-\gamma}}. \quad (67)$$

Putting these expressions in Eq. (62) we find the following implicit equation for q_c :

$$\frac{\gamma - 2}{\gamma - 3} \frac{m^{3-\gamma} - \zeta^{3-\gamma}}{m^{2-\gamma} - k_{\max}^{2-\gamma}} - \frac{m^{2-\gamma} - \zeta^{2-\gamma}}{m^{2-\gamma} - k_{\max}^{2-\gamma}} = 1. \quad (68)$$

Equation (68) simplifies considerably when $k_{\max} \rightarrow \infty$. Indeed (for $\gamma \geq 2$), we find the same result as in [10]:

$$\frac{\gamma - 2}{\gamma - 3} \left(m - \frac{\zeta^{3-\gamma}}{m^{2-\gamma}} \right) + \frac{\zeta^{2-\gamma}}{m^{2-\gamma}} = 2. \quad (69)$$

Considering the ensemble where $k_{\max} = mN^{1/(\gamma-1)}$, when $N \rightarrow \infty$ then $k_{\max} \rightarrow \infty$, the relation between ζ and q_c is $\zeta = m q_c^{1/(1-\gamma)}$, and we finally find:

$$q_c^{(2-\gamma)/(1-\gamma)} = 2 + \frac{\gamma - 2}{\gamma - 3} m (q_c^{(3-\gamma)/(1-\gamma)} - 1), \quad (70)$$

which is the known result for the HD attack [10]. The solution is shown in Extended Data Fig. 1a.

For $\gamma = 2$, Eq. (70) predicts a zero critical q_c for any m , and this is interpreted as an extreme fragility of scale-free networks when the degree exponent is close to 2. Indeed, for $\gamma = 2$, the network is essentially a star-graph, which is trivially destroyed by removing the central hub. This in turn is a consequence of the fact that the natural cut-off k_{\max} diverges linearly with the system size for $\gamma = 2$, i.e., $k_{\max} \sim N$ (see Extended Data Fig. 1a).

Nonetheless the situation changes a lot for other network ensembles, where the cut-off can be very large but finite (which is the case of all networks, both real and synthetic ones). Indeed, Eq. (68) for a finite cut-off k_{\max} and for $\gamma \rightarrow 2$ gives:

$$\zeta = m + \log \left(\frac{\zeta k_{\max}}{m^2} \right). \quad (71)$$

By expressing ζ as a function of q_c via the equation:

$$\zeta = \frac{mk_{\max}}{m + q_c(k_{\max} - m)}, \quad (72)$$

we find the equation for q_c as a function of the cut-off k_{\max} :

$$\frac{mk_{\max}}{m + q_c(k_{\max} - m)} = m + \log \frac{k_{\max}^2}{m^2 + mq_c(k_{\max} - m)}. \quad (73)$$

The solution to Eq. (73) is shown in Extended Data Fig. 1b. For $k_{\max} \rightarrow \infty$, the asymptotic behaviour of the threshold q_c is given by :

$$q_c \sim \frac{m}{\log(k_{\max})} \quad \text{for } k_{\max} \rightarrow \infty. \quad (74)$$

Therefore, q_c still vanishes when $k_{\max} \rightarrow \infty$ but as the inverse of the logarithm of the cut-off. This very slow convergence makes questionable the claim that scale free networks are extremely fragile under hubs removal. Indeed, as can be seen in Extended Data Fig. 1b, even for k_{\max} of the order of hundred millions, q_c is still of order 0.1. For more realistic $k_{\max} = 10^3$, which is typical of social networks, $q_c \approx 0.2$ for all γ . In these situations, the search for other attack strategies becomes important.

III. OPTIMIZATION WITH THE CAVITY METHOD

The eigenvalue $\lambda(\mathbf{n})$ can be minimized by using the cavity method from spin glass theory [28] since we work with sparse graphs. The method can be applied in practice to the first order approximation to the eigenvalue $\ell = 1$, which is a pair-wise interaction, i.e., Eq. S40:

$$\lambda_1(\mathbf{n}) = \frac{|\mathbf{w}_1(\mathbf{n})|}{|\mathbf{w}_0|}. \quad (75)$$

For higher order many-body interactions, the cavity method becomes much more involved and we will pursue other solving strategies.

The analytical Replica Symmetry (RS) solution obtained with the cavity method for this pairwise model allows us to compare with the solution given by EO. This is a very useful check of the correctness of the problem solution, since both method are mathematically not rigorous. An improvement over the RS solution can be obtained by applying the so called 1step replica symmetry breaking cavity method (1RSB) [28, 36], which should be compared as well with the EO solution. This will be done in a future work. Here we only note that,

as far as the assessment of the ground state energy is concerned, the difference between the RS and the 1RSB estimations is, typically, very small (for example it is less than 2% for spin glass models on random graphs [36]). We expect that the same scenario holds true also for the model defined here. Furthermore, a deeper physical insight can be obtained when we recast the problem in terms of spin glass theory as we show next.

The energy (cost) function of the problem is, Eq. S39:

$$\mathcal{E}(\mathbf{n}) \equiv |\mathbf{w}_1(\mathbf{n})|^2 = \sum_{ij} A_{ij}(k_i - 1)(k_j - 1)n_i n_j . \quad (76)$$

The physics of this system is made more transparent when the problem is formulated in terms of Ising spin variables $s_i = \pm 1$. The translation of the problem in the language of statistical mechanics will turn the optimization problem to one of finding the ground state of a spin-glass system. The relation between s_i and n_i is given by

$$s_i \equiv 2n_i - 1. \quad (77)$$

Note that the state $n_i = 0$, meaning that node i is removed (influencer), corresponds to the spin down state $s_i = -1$. On the other hand the state $n_i = 1$ (node i not removed) corresponds to spin up $s_i = 1$. Using these new variables the energy function takes the more familiar form of an Ising model:

$$\mathcal{E}(\mathbf{s}) = - \sum_{\langle ij \rangle} s_i J_{ij} s_j - \sum_i H_i s_i + \mathcal{C} , \quad (78)$$

where the first sum on the r.h.s is over the pairs $\langle ij \rangle$ of nearest neighbours sites in the network. The coupling constants J_{ij} represent the interactions between the spins and they depend on the details of the network. Explicitly they read:

$$J_{ij} = -\frac{1}{2} A_{ij}(k_i - 1)(k_j - 1) . \quad (79)$$

The local field H_i depends also on the topology and is given by:

$$H_i = -\frac{1}{2} k_i(k_i - 1)(k_i^{nn} - 1) , \quad (80)$$

where k_i^{nn} is the average nearest neighbors degree of vertex i , defined as:

$$k_i^{nn} \equiv k_i^{-1} \sum_{j \in \partial i} k_j . \quad (81)$$

The constant \mathcal{C} does not depend on the spin variables and can be ignored in the minimization problem (but must be included in the evaluation of the energy $\mathcal{E}(\mathbf{s})$).

We introduce also the magnetization,

$$m \equiv \sum_i s_i / N, \quad (82)$$

of the configuration \mathbf{s} , which is related to the number of removed nodes q by the equation

$$m \equiv 1 - 2q. \quad (83)$$

Note that $\mathcal{E}(m = -1) = 0$, and $\mathcal{E}(m = +1) = \langle k \rangle (\kappa - 1)^2$ (for uncorrelated networks), where $\kappa = \langle k^2 \rangle / \langle k \rangle$.

The physical system defined by the energy function (78) is a disordered antiferromagnet ($J_{ij} \leq 0$) in a random external magnetic field. Remarkably, the disorder in the model, J_{ij} , comes from the randomness in the network via the adjacency matrix A_{ij} , even if for a given instance of the problem both the couplings and the magnetic field are deterministic (i.e. fixed by the topology of the underlying network and the degree).

The problem we have to solve is tantamount to find the ground state of the system with energy function (78). More precisely, we want to find the ground state for a fixed value of the magnetization m , which corresponds to keep fixed the number of removed nodes q . This problem represents a quite novel system for spin glass theory since the coupling J_{ij} depends explicitly on the contact network via Eq. S79. This coupling between the underlying network and the disorder is a quite unique feature of the optimal percolation problem at the $\ell = 1$ pair-wise level. The problem becomes spin-glass when the system is forced to satisfy a given magnetization, i.e., a given fraction of influencers, which is a global constraint. This additional constraint of constant magnetization represents a problem for the cavity method, since it cannot be enforced locally. Nevertheless the problem can be circumvented by introducing an external field H that is chosen self-consistently to fix the desired value of the magnetization as done in [43]. In practice, we introduce the Legendre transform of the energy function $\mathcal{E}(\mathbf{s})$, defined as

$$\begin{aligned} E_H(\mathbf{s}) &= \mathcal{E}(\mathbf{s}) - MH, \\ \frac{\partial E_H}{\partial H} &= -M, \end{aligned} \quad (84)$$

where $M = \sum_i s_i$ is the global magnetization. At this point we have to minimize the function $E_H(\mathbf{s})$ under the global constraint defined by the equation $\partial E / \partial H = -M$. This can be done

by properly gauging the external field H during the iteration of the cavity equations, as we will explain below.

The cavity equations for the system defined by the energy function $E_H(\mathbf{s})$ are a set of equations for the cavity fields $h_{i \rightarrow j}$ and the cavity bias $u_{i \rightarrow j}$, one for each directed edge of the graph. These variables can be interpreted as messages exchanged by the nodes: the bias $u_{i \rightarrow j}$ represents the incoming message into node j traveling along the edge connecting i and j ; the field $h_{i \rightarrow j}$ is the outgoing message from node i towards node j . Outgoing messages are computed from the incoming ones in a self-consistent way. The cavity field $h_{i \rightarrow j}$ quantifies the tendency of spin i to be $+1$ or -1 , when the spin on node j has been pruned from the network (whence the name cavity). The cavity bias $u_{i \rightarrow j}$ is determined by optimizing between the interaction J_{ij} and the cavity field $h_{i \rightarrow j}$. More precisely, the cavity equations for cavity bias and cavity fields at zero temperature read:

$$\begin{aligned} h_{i \rightarrow j} &= H(M) + H^i + \sum_{k \in \partial i \setminus j} u_{k \rightarrow i} , \\ u_{k \rightarrow i} &= \frac{1}{2} \text{sign}(J_{ik} h_{k \rightarrow i}) \min(|J_{ik}|, |h_{k \rightarrow i}|) . \end{aligned} \tag{85}$$

Once a solution of the cavity equations (85) has been found, the total local effective field h_i acting on spin i can be computed through the formula:

$$h_i = H(M) + H^i + \sum_{k \in \partial i} u_{k \rightarrow i} \tag{86}$$

The main hypothesis of the cavity method is the existence of a single pure state, which can be rephrased as a hypothesis on the uniqueness of the solution of the cavity equations (85). This is called the replica-symmetric (RS) cavity method. It is also possible to generalize the method to incorporate multiple solutions (the so called cavity method at the level of 1step Replica Symmetry Breaking, 1RSB [28]). The analysis of this second method will come in a follow-up work. Here we limit ourselves to the RS cavity method.

The cavity equations (85) can be interpreted as updating rules for a message passing algorithm, and therefore they can be solved iteratively starting from a random initial condition. In practice we add a "time" label t to the cavity fields and we rewrite Eqs. (85) as dynamical message passing equations:

$$h_{i \rightarrow j}^{(t)} = H(M) + H^i + \sum_{k \in \partial i \setminus j} u_{k \rightarrow i}^{(t-1)} . \tag{87}$$

Since the magnetization M has to be kept fixed, the external field $H(M)$ also needs to be updated at each step of the iteration. Therefore, after a total update of the cavity fields $h_{i \rightarrow j}^{(t)}$, the field $H(M) \equiv H^{(t)}(M)$ is recomputed by solving the equation:

$$\sum_i \text{sign} \left(H^{(t)}(M) + H^i + \sum_{k \in \partial i} u_{k \rightarrow i}^{(t)} \right) = M. \quad (88)$$

The solution of the Eqs. (85) corresponds to the fixed point of the map defined by Eqs. (87) and (88).

Once the solution of the cavity equations has been found, the RS estimate of ground state energy E_H^{RS} is given by:

$$E_H^{\text{RS}} = \sum_i \epsilon_H^i - \sum_{(ij)} \epsilon_{ij}, \quad (89)$$

where the site and link energies ϵ_H^i and ϵ_{ij} are given, respectively, by

$$\begin{aligned} \epsilon_H^i &= - \max \left(H(M) + H^i + \sum_{k \in \partial i} |h_{k \rightarrow i} + J_{ik}|, \right. \\ &\quad \left. -H(M) - H^i + \sum_{k \in \partial i} |h_{k \rightarrow i} - J_{ik}| \right), \\ \epsilon_{ij} &= - \max (h_{i \rightarrow j} + J_{ij} + h_{j \rightarrow i}, h_{i \rightarrow j} - J_{ij} - h_{j \rightarrow i}, \\ &\quad -h_{i \rightarrow j} - J_{ij} + h_{j \rightarrow i}, -h_{i \rightarrow j} + J_{ij} - h_{j \rightarrow i}) . \end{aligned} \quad (90)$$

From the knowledge of the function E_H^{RS} we can compute the energy $\mathcal{E}_M^{\text{RS}}$ by inverting the Legendre transform:

$$\mathcal{E}_M^{\text{RS}} = E_H^{\text{RS}} + MH(M), \quad (91)$$

where $H(M)$ is the external field which produces the desired value of the magnetization M , given by the fixed point of Eq. (88). The value of $\mathcal{E}_M^{\text{RS}}$ is all we need to compute the optimized eigenvalue. Since $|\mathbf{w}_0| = \sqrt{N \langle k \rangle}$, we finally find:

$$\lambda_1^{\text{RS}}(m) = \sqrt{\frac{\epsilon^{\text{RS}}(m)}{\langle k \rangle}}, \quad (92)$$

where $\epsilon^{\text{RS}}(m) = \mathcal{E}_M^{\text{RS}}/N$ is the (intensive) energy per spin.

We observed that the message passing equations (87) never converge to a stable fixed point. This is a consequence of the existence of very many solutions to the cavity equations

(85), which implies that the replica symmetry is broken for this system. Nevertheless, the non-converged messages can still be used to estimate the energy $\epsilon^{\text{RS}}(m)$. In practice we run the algorithm for a maximum number of $T_{\text{max}} = 10^6$ iteration. Then we use the current value of the cavity fields $\{h_{i \rightarrow j}\}$ to compute the energy of the system, and we average the energy on T_{max} more iterations.

In Extended Data Fig. 2 we show the optimized eigenvalue λ_1^{RS} as a function of the removed nodes $q = 1 - 2m$, computed for an Erdős-Rényi network with mean degree $\langle k \rangle = 3.5$ and size $N = 10^4$. We find the transition point at this 2-body interaction approximation to be $q_c = 0.248$.

The continuous transition from the phase with $\lambda_1^{\text{RS}} = 0$ to the phase with $\lambda_1^{\text{RS}} > 0$ observed in Extended Data Fig. 2 is an artifact of the 2-body interaction considered here. Indeed the real optimal eigenvalue (i.e. the eigenvalue including ∞ -body interactions) has to jump from zero to one discontinuously at q_c as depicted in Fig. 1c. The reason is that the largest eigenvalue of the non-backtracking matrix of a tree-graph is zero, while the largest eigenvalue for a tree plus one single loop is one. Adding more loops increases the eigenvalue. Since there are no other possible networks between a tree and a unicyclic graph, the largest eigenvalue of the non-backtracking matrix cannot take values in the interval $(0, 1)$. As a consequence it has to jump discontinuously from 1 to zero at q_c . In the 2-body approximation this jump is smoothed by a continuous line. By considering higher order interactions the eigenvalue would remain zero closer and closer to the critical threshold q_c . This is evident, for example, in the problem with 3, 4 and 5 interactions, that we solve using extremal optimization next. We expect that adding more and more interactions the eigenvalue has several (continuous) transitions, when departing from zero, for smaller and smaller values of q and eventually for interactions of infinite order it jumps discontinuously from zero to one exactly at q_c .

In the inset of Extended Data Fig. 2 we show also a comparison between the RS cavity method and extremal optimization done in the next section. As can be seen the difference is very small, and we believe that they are actually very close to the true optimal result. The size of the ER network in this case is $N = 128$, for which EO gives the actual ground state. In favor of this conjecture we can also say that the 1RSB estimate, which is in general more correct than the RS one, is anyway very close to the latter, and would lie in between of the two curves shown in the inset of Extended Data Fig. 2. The eigenvalue estimated

with RS is anyway slightly smaller. This is a typical feature of the RS cavity method, in the sense that it gives a lower bound (and not an upper bound) to the ground state energy of the system. On the contrary, EO provides an upper bound to the optimal threshold. As the inset of Extended Data Fig. 2 shows, both the lower bound (RS) and the upper bound (EO) are very close to each other, and therefore to the true optimum. Therefore, we observe that there can be different ways to analytically assess the location of the optimal threshold. Conversely, this does not mean that different methods are equally able to find the actual configuration of optimal influencers, even if they give similar analytical estimation for the threshold. A more important issue in any NP problem, perhaps the most relevant for any practical purpose, is finding a scalable algorithm which approximates the optimal configuration as better as possible and can be used for very large networks. This is the main reason why our CI algorithm was designed for.

To conclude this section we want to observe that the antiferromagnetic nature of the optimal percolation problem is not totally unexpected. Indeed, the antiferromagnetic interactions between nodes reflect the intuitive idea that immunizing contiguous nodes is less efficient than immunizing them in a staggered way.

IV. MINIMIZATION WITH EXTREMAL OPTIMIZATION (EO)

In this section we describe another method for the minimization of the eigenvalue $\lambda(\mathbf{n})$, called Extremal Optimization (EO) [29], which has the advantage, with respect to the cavity method, to be easily implemented for higher ℓ -order of $|\mathbf{w}_\ell(\mathbf{n})|$. However, EO is still not scalable for large networks, for which we will implement CI. Nevertheless, EO makes use of the full energy function, including loops, and can be used to extrapolate the solution for large networks where EO is not applicable anymore. Indeed, the EO algorithm is an efficient method to find nearly optimal solutions. It was used successfully to find the ground state energy of spin glass models on random graphs, where it was shown to be practically identical to the best available analytical prediction [29]. We believe that also in our case τ -EO is very close to the optimum when extrapolated to large systems. In Extended Data Figs 3 and 4 we estimate the optimal solution for large networks using a finite size scaling analysis extrapolating to the infinite size limit and $\ell \rightarrow \infty$, as explained next.

To explain the method in the simplest way let us consider again the lowest non trivial

approximation to the eigenvalue $\lambda(\mathbf{n}) \sim \frac{|\mathbf{w}_1(\mathbf{n})|}{|\mathbf{w}_0(\mathbf{n})|}$ and the corresponding cost function $\mathcal{E}(\mathbf{n})$:

$$\mathcal{E}(\mathbf{n}) \equiv |\mathbf{w}_1(\mathbf{n})|^2 = \sum_{ij} A_{ij}(k_i - 1)(k_j - 1)n_i n_j. \quad (93)$$

We now assign to each variable n_i the fitness b_i :

$$b_i = (k_i - 1) \sum_j A_{ij}(k_j - 1)n_j, \quad (94)$$

so that we can rewrite the energy function (93) as

$$\mathcal{E}(\mathbf{n}) = \sum_i b_i n_i. \quad (95)$$

Notice that this is similar to the form we adopt to define CI in Eq. (5). The CI-algorithm is an adaptive version of the EO algorithm, in a sense that will be explained in Sec. V. The EO algorithm being the exact minimization of the largest eigenvalue of the NB matrix, which can only be achieved for small systems.

Each node in the state $n_i = 0$ (removed) gives zero contribution to the energy, while nodes for which $n_i = 1$ give a contribution equals to their fitness. Therefore, to minimize the energy $\mathcal{E}(\mathbf{n})$ we have to find the set of nodes with the lowest fitness, under the usual constraint $\sum_i n_i = N(1 - q)$. Note that the fitness b_i of node i depends on the states n_j of its neighbours j .

The aim of EO is to explore the space of states looking for the configurations with the smallest fitness. Let now explain how it works. For a fixed q , in the beginning the variables n_i are assigned at random into two sets: set S_0 containing the qN nodes to be removed $n_i = 0$, and set S_1 containing $(1 - q)N$ nodes with $n_i = 1$:

$$\begin{aligned} S_1 &\equiv \{i : n_i = 1\}, \\ S_0 &\equiv \{i : n_i = 0\}, \end{aligned} \quad (96)$$

with the constraints $|S_0| = Nq$, and $|S_0| + |S_1| = N$. The initial separation of the nodes in these two groups is made arbitrarily. Then the fitness b_i corresponding to this initial configuration C_0 are evaluated and sorted separately for the two groups. The first move consists in exchanging the variable n_i in S_1 with the largest fitness, with the variable n_j in S_0 with the lowest one. In other words, we set $n_i = 0$ and $n_j = 1$. This move does not change the sizes of S_1 and S_0 and hence the global constraint $\sum_i n_i = N(1 - q)$ remains

satisfied. The energy function (95) corresponding to this new configuration C_1 is evaluated and if $\mathcal{E}(C_1) < \mathcal{E}(C_0)$ the configuration C_1 is stored together with the value of its energy. The process is repeated by recomputing the new fitness and swapping the variable with the highest value of b_i from S_1 with the variable corresponding to the lowest one in S_0 . Note that the moves are accepted unconditionally at each step and only the best configuration found so far is saved. The algorithm is terminated after a maximum number of iteration is reached.

What we have described so far is the basic EO algorithm. It can be improved by introducing a tunable parameter, called τ , so that we will refer to it as τ -EO. In this version of the algorithm, the choice of the variables to be swapped is not performed deterministically by selecting the ones with the largest and smallest fitness, but, instead, they are picked up using a random selection. This may look counterintuitive at first sight, since we would not expect any improvement by randomizing the choice. Actually this is not true, and an improvement can be achieved, provided that the random rule is chosen judiciously.

In the τ -EO algorithm, we sort the fitness in the two sets S_0 and S_1 , in increasing order in S_1 and decreasing order in S_0 :

$$\begin{aligned} b_{\Pi(1)} &\geq b_{\Pi(2)} \geq \dots \geq b_{\Pi(|S_1|)} , \\ b_{\Lambda(1)} &\leq b_{\Lambda(2)} \leq \dots \leq b_{\Lambda(|S_0|)} , \end{aligned} \tag{97}$$

where Π and Λ are two permutations of the labels i of the variables in S_1 and S_0 respectively. The worst variable in S_1 (the one with the highest fitness) is $n_{\Pi(1)}$, that we want to change with the worst variable in S_0 , i.e., $n_{\Lambda(1)}$ (the one with the lowest fitness). In the simple EO algorithm this is exactly what we were doing: exchanging $n_{\Pi(1)}$ and $n_{\Lambda(1)}$. Now we rank the variables according to their fitness.

For the variables in S_1 the worst variable is $n_{\Pi(1)}$, which has rank 1, while the best variable is $n_{\Pi(|S_1|)}$, which is of rank $|S_1|$. For the variables in S_0 the variable of rank 1 is $n_{\Lambda(1)}$, while $n_{\Lambda(|S_0|)}$ has rank $|S_0|$. Then we consider the following probability distribution over the ranks r :

$$P(r) \propto r^{-\tau} , \tag{98}$$

with $r \in [1, |S_1|]$ or $r \in [1, |S_0|]$ for the ranks of variables in S_1 or S_0 , respectively. At each update, we draw two numbers r_1 and r_0 from $P(r)$ and then we swap the variables $n_{\Pi(r_1)}$ and $n_{\Lambda(r_0)}$. Then the algorithm proceeds as in the original EO. Note that for $\tau \rightarrow \infty$, we

recover the deterministic EO algorithm, swapping only the worst variables. The idea behind the choice of the scale free distribution $P(r)$ is to ensure that no variable gets excluded from changing set, while giving higher priority to the variables with worst fitness. The random selection of the variables has the advantage, over the deterministic process, to make possible global reconfigurations of the system, thus climbing over the energy barriers and find better minima. In our problem we found that a value of $\tau = 1.7$ gives the best results.

As an application of this method, we perform the minimization of the energy function $\mathcal{E}(\mathbf{n})$ on an Erdős-Rényi network with average degree $\langle k \rangle = 3.5$. We considered different system sizes $N = 2^5, 2^6, 2^7, 2^8$. For each size N we took the average of the ground state energy over 100 realizations. For each instance we performed N^3 updates of the τ EO routine. The results for the eigenvalue $\lambda(q) = \sqrt{\mathcal{E}(q)/N\langle k \rangle}$ are shown in Extended Data Fig. 3.

We observe that the finite size scaling of the optimal influence threshold q_c , which is the solution of $\lambda(q_c) = 1$, is consistent with the scaling law:

$$q_c(N) = q_c(\infty) + AN^{-2/3}, \quad (99)$$

where A is a coefficient independent from the size N . This scaling form is the same of the finite size correction to the thermodynamical energy density of a spin glass system with pairwise interactions (e.g. the SK model) at and below the de Almeida-Thouless line. Actually this scaling form is observed also for other interesting thermodynamic quantities, like the second cummulant of the overlap distribution [44]. In that case the anomalous scaling (as opposed to the more natural $1/N$ correction expected from the central limit theorem) is due to the existence of infinitely many zero modes, whose volume grows as $N^{1/3}$. In the language of our model, these zero modes represent the infinitely many way to choose the set of optimal influencers. It would be very interesting then to interpret what kind of hidden symmetry relates all these set of optimal influencers.

A. τ -EO with multibody interactions

In the general case the energy function we want to minimize is:

$$\mathcal{E}(\mathbf{n}) = |\mathbf{w}_\ell(\mathbf{n})|^2 \quad (100)$$

which involves at most 2ℓ -body interactions. To treat systems with at most a (odd) number of $(2\ell + 1)$ -body interactions, we consider the energy function:

$$\mathcal{E}'(\mathbf{n}) = \langle \mathbf{w}_\ell(\mathbf{n}) | \hat{\mathcal{M}} | \mathbf{w}_\ell(\mathbf{n}) \rangle . \quad (101)$$



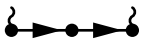


In order to apply the EO algorithm to systems with many-body interactions, all that we have to do is to change the definition of the fitness b_i . For example, in the case of a system with 4-body interactions, described by $|\mathbf{w}_2(\mathbf{n})|^2$, we set b_i as:

$$b_i = \sum_{jk\ell} A_{ij} A_{jk} A_{k\ell} (1 - \delta_{ik})(1 - \delta_{j\ell}) z_i z_\ell n_j n_k n_\ell, \quad (102)$$

where $z_i = k_i - 1$.

After that, the algorithm can be applied exactly in the same way as we did for the system with two body interactions. We use the algorithm to minimize the energy function of a system with 3, 4, 5-body interactions as shown in Extended Data Fig. 3. Two comments are in order. Firstly, we note that the eigenvalue is zero for a larger interval of values of q with respect to the one computed in the system with 2-body interactions. This observation corroborates the idea that in the limit of infinitely many interactions the eigenvalue jumps at q_c from zero to one.

In Extended Data Fig. 4a we show the threshold $q_c(N)$ as a function of the system size for different values of the order of the many-body interactions ρ . The thermodynamic limit for each many-body interaction $q_c^\infty(\rho)$ is obtained by $N \rightarrow \infty$ (the y -intercept in the figure). The value at $\rho = 1$ represents the system with one-body interaction (equivalent to HD). The value $\rho = 2$ represents the system with 2-body interactions and energy function $|\mathbf{w}_1(\mathbf{n})|^2$; $\rho = 3$ corresponds to the system with (at most) 3-body interactions and energy $\langle \mathbf{w}_1(\mathbf{n}) | \mathcal{M} | \mathbf{w}_1(\mathbf{n}) \rangle$, as summarized in the following Table for the first three levels.

	Even interactions	Odd interactions
Energy function	$\mathcal{E}_\ell(\mathbf{n}) = \mathbf{w}_\ell(\mathbf{n}) ^2$	$\mathcal{E}'_\ell(\mathbf{n}) = \langle \mathbf{w}_\ell(\mathbf{n}) \hat{\mathcal{M}} \mathbf{w}_\ell(\mathbf{n}) \rangle$
Order of Interactions	$\rho = 2\ell$	$\rho = 2\ell + 1$
Leading diagram for $\ell = 0$		 one-body
Leading diagram for $\ell = 1$	 two-body	 three-body
Leading diagram for $\ell = 2$	 four-body	 five-body

In Extended Data Fig. 4b, we extrapolate the infinite size threshold $q_c^\infty(\rho)$ to the limit of ∞ -body interactions, i.e., for $\rho \rightarrow \infty$. The scaling of q_c^∞ with $1/\rho$ is well consistent with a linear behaviour. We obtain the $\rho = \infty$ limit of $q_c^\infty(\rho = \infty) \equiv q_c^{\text{opt}}$ from a least-squares fit. For ER networks with average degree $\langle k \rangle = 3.5$ studied here, we find $q_c^{\text{opt}} = 0.192(9)$. This is the value of the optimal threshold shown in Fig. 2a in the main text.

V. CI ALGORITHM

We have shown so far that the problem of finding the optimal set of influencers can be solved by minimizing the following cost function which is the leading order approximation in $1/N$:

$$E_\ell(\mathbf{n}) = \sum_{i=1}^N z_i \sum_{j \in \partial \text{Ball}(i, \ell)} \left(\prod_{k \in \mathcal{P}_\ell(i, j)} n_k \right) z_j, \quad (103)$$

where $E_\ell(\mathbf{n}) = |\mathbf{w}_{(\ell+1)/2}|^2$ for ℓ odd (corresponding to the energy function $\mathcal{E}(\mathbf{n})$ in Eq. S100), and $E_\ell(\mathbf{n}) = \langle \mathbf{w}_{\ell/2} | \hat{\mathcal{M}} | \mathbf{w}_{\ell/2} \rangle$ for ℓ even (corresponding to $\mathcal{E}'(\mathbf{n})$ in Eq. S101). We recall that $z_i = k_i - 1$. We define the collective influence strength at level ℓ , of node i as:

$$\text{CI}_\ell(i) = z_i \sum_{j \in \partial \text{Ball}(i, \ell)} \left(\prod_{k \in \mathcal{P}_\ell(i, j)} n_k \right) z_j, \quad (104)$$

and we can rewrite Eq. (103) as:

$$E_\ell(\mathbf{n}) = \sum_{i=1}^N \text{CI}_\ell(i). \quad (105)$$

Notice that $\text{CI}_\ell(i)$ is basically the same as the fitness b_i of the EO algorithm, and precisely: $\text{CI}_\ell(i) = b_i n_i$. A fast and efficient way to minimize the cost function $E_\ell(\mathbf{n})$ is to adaptively remove the nodes with the highest collective influence $\text{CI}_\ell(i)$. When all the nodes are present, corresponding to $\mathbf{n} = \mathbf{1}$, $\text{CI}_\ell(i)$ evaluates:

$$\text{CI}_\ell(i) = z_i \sum_{j \in \partial \text{Ball}(i, \ell)} z_j. \quad (106)$$

This is the expression of $\text{CI}_\ell(i)$ given in the main text Eq. (5). By computing this quantity for each node, we can find the one with the largest collective influence and then remove it. We stress that the frontier of the Ball: $\partial \text{Ball}(i, \ell)$ consists of all the nodes j that

are at a distance ℓ from i , the distance is measured as the minimum path between i and j . This definition is consistent with the fact that we have neglected the NB walks with loops in the definition of the energy functional Eq. S53 for large networks, and therefore also in $\text{CI}_\ell(i)$ Eq. S106, since they scale as $O(1/N)$ in random networks as discussed in Section II F.

After the removal, the network consists of $N - 1$ nodes, and we can proceed as before, looking for the next node with the largest CI_ℓ . Since the removal of the first node changes the degree of its neighbours, we need to decrease their degrees by one before recomputing their CI_ℓ . Removing one by one the nodes according to this adaptive principle we can destroy the network in a nearly optimal and very fast way. Besides, we can significantly speed up the algorithm by decimating a finite fraction of nodes at each step (see Section V B). The algorithm's performance increases by using larger values of the radius ℓ of the $\text{Ball}(i, \ell)$. In Extended Data Fig. 5 we show the results for different values of ℓ . We observe that already for $\ell = 3, 4$ the algorithm reaches the top performance.

When ℓ becomes larger than the network diameter, then $\text{CI}_\ell(i) = 0$. In this situation different nodes are not distinguishable by the algorithm, and thus, the method is basically indistinguishable from a random one. Thus, the parameter ℓ should not exceed in practice the original network diameter. We also notice that dangling ends give zero contribution by CI, and hence they are ignored by the algorithm. This is expected since dangling ends should have zero influence in the network.

The CI algorithm Eq. (5) is based on Eq. (4) which contains the many-body collective interactions that we refer to as “collective influence”. The CI algorithm incorporates the collective effects by considering the adaptive nature of the algorithm. The adaptiveness of the CI algorithm, usually called decimation in the spin glass literature [36], is a collective way to select influential nodes, since the removal of each node depends heavily on the history of the process.

A. Optimization for $G(q) \neq 0$

The theory we developed for the optimal fragmentation of networks allows us to compute the optimal influence threshold q_c , i.e. the smallest number of nodes to remove such that $G(q_c) = 0$, together with the corresponding configuration \mathbf{n}^* .

When $q < q_c$ the giant component is nonzero, a consequence of the fact that the system of Eqs. (9) has another stable solution different from $\{\nu_{i \rightarrow j}\}$ identically zero. Therefore, for $q < q_c$ the stability of the new solution $G(q) \neq 0$ is no more controlled by the non-backtracking operator, but a more complicated operator comes into play that depends on the form of the solution itself. To find the spectrum (or even the largest eigenvalue) of this new matrix we have necessarily to know the solution of the problem. This circumstance depauperates the method of its power in $q < q_c$, since we need the solution to the problem to solve the problem itself. In the regime $q > q_c$, where $G(q) = 0$, this solution can be easily guessed, as we did, but for $q < q_c$ no simple ansatz can be adopted.

What can we do in the regime $q < q_c$ to minimize the size of the giant component?

We know that the configuration \mathbf{n}^* corresponds to a zero giant component. Assuming that this configuration is the optimal one (this hypothesis is not crucial in what follows and can be relaxed by saying that \mathbf{n}^* is the best approximation to the true optimum), then the optimal trajectory in the configuration space, starting from the point $\mathbf{n} = (1, 1, 1, \dots, 1)$ corresponding to $q = 0$ and $G(0) = 1$, must end up at the point \mathbf{n}^* at $q = q_c$ where $G(q_c) = 0$.

So far we know the final point \mathbf{n}^* and we would like to travel back the optimal trajectory up to the initial point $\mathbf{n} = \mathbf{1}$. In order to do that, let us suppose to decrease infinitesimally the fraction of removed nodes q from its critical value q_c , that is $q = q_c - dq$ [dq can be taken equal to $1/N$, so that $Ndq = O(1)$]. This amounts to explore a neighborhood of the configuration \mathbf{n}^* , consisting of a collection of configurations \mathbf{n}' in which a number Ndq of components $n'_i = 0$ is turned into $n'_i = 1$. Here we are making the crucial hypothesis that the optimal trajectory is continuous, in the sense that in going from $q \rightarrow q - dq$ only a number Ndq of components n_i is changing state. Under this assumption the trajectory can be followed adiabatically up to the point $\mathbf{n} = \mathbf{1}$.

Mathematically, this can be expressed by saying that the Hamming distance between two neighbouring optimal configurations \mathbf{x} and \mathbf{y} : $d(\mathbf{x}, \mathbf{y}) = \sum_{i=1}^N |x_i - y_i|$, is equal to $d(\mathbf{x}, \mathbf{y}) = Ndq$. This hypothesis may not hold in the case where the optimal configuration \mathbf{x} corresponding to Nq removed nodes, and the one \mathbf{y} corresponding to $N(q - dq)$ have an Hamming distance much larger than Ndq . In this case the optimal trajectory has discontinuities, jumping from one point to another which are not close to each other. Physically this correspond to the fact that the optimal state \mathbf{y} cannot be obtained from the optimal state \mathbf{x} by flipping a finite number of components n_i , but requires a global rearrangement of the sys-

tem, which amounts to change the state of much more variables n_i , whose number scales as N^α with exponent $\alpha \in (0, 1]$. This situation takes place in spin-glass systems with Full-RSB thermodynamics, where this chaotic behaviour is observed as a function of the temperature [45] (or as a function of other control parameters like the bond strengths and the magnetic field). In that case, when the system is cooled from a temperature T to $T - dT$ (with T below the critical point: $T < T_c$), the Gibbs state corresponding to the higher temperature does not survive after the cooling, but, instead, a completely new equilibrium state appears at $T - dT$ (i.e. if we sample a typical equilibrium configuration at temperature T , this will be very distant, in the Hamming sense, from a configuration sampled at $T - dT$).

It is highly plausible that the same situation (a chaotic trajectory) is realized also in our problem. To keep things simple, we don't explore this scenario, and analyze only the consequences deriving from the hypothesis of a smooth optimal trajectory from \mathbf{n}^* back to **1**. This approach will give us a very efficient algorithm to minimize the giant component in all the interval $q \in [0, q_c)$, at no additional computational cost. Therefore we take this performance as a practical justification of the main assumption, leaving to a future work the treatment of the more complicated chaotic scenario.

To take up the threads of our discussion, let us assume that optimal configurations lie close to each other. Knowing the optimal configuration at the fraction q , we should be able to find the new optimal one at $q - dq$ by changing the state of few variables, and actually only one if we take $dq = 1/N$. Practically we have to find the new optimal configuration by changing the state of a single variable from 0 to 1. Practically we proceed in the following way. At $q = q_c$, we have $G(q_c) = 0$. The corresponding configuration n^* contains Nq_c variables $n_i = 0$ (removed nodes), and $N(1 - q_c)$ variables $n_i = 1$ (nodes that are present). At this point we start to add back to the network the nodes using the following algorithm. We assign to each removed node $n_i = 0$ an index $c(i)$, which is calculated as the number of clusters that node i would join if it were reinserted in the network, independently of their sizes. Then we put back in the network node i^* such that $i^* = \operatorname{argmin}_{n_i:n_i=0} c(i)$, by changing $n_i^* = 0$ into $n_i^* = 1$ (see Extended Data Fig. 6). The idea behind this method is the fact that we want to keep a maximally fragmented network after each reinsertion of nodes. We keep on reinserting nodes using the same criterion, until no node is left for which $n_i = 0$. After each reinsertion the indexes $c(i)$ are recalculated, and then the new node with minimum $c(i)$ is chosen.

The running time of this algorithm is $O(MN \log N)$, where M is the number of edges. Indeed, $O(M)$ operations are needed to assign the indexes $c(i)$ and $O(N \log N)$ to sort them. As we did for the case of the main CI algorithm, the time complexity of this algorithm can be reduced to $O(N \log N)$ (if $M = O(N)$), by reinserting a finite fraction of nodes at time.

B. Scalability of the CI algorithm

The time complexity needed to compute the quantity $CI_\ell(i)$ is proportional to the number of edges inside the ball $\text{Ball}(i, \ell)$. Since the radius ℓ is taken finite, this calculation takes a time $O(1)$ for each node (even if the prefactor increases with ℓ). Thus, to compute the $CI_\ell(i)$ for all i requires $O(N)$ operations. Sorting the $CI_\ell(i)$'s takes $O(N \log N)$. The algorithm is terminated when a number Nq_c of nodes is removed. Therefore, removing the nodes one-by-one, the total time complexity would be $O(N^2 \log N)$. Actually we can keep the computational complexity to $O(N \log N)$ without losing any performance, by simply removing a finite fraction of nodes at each step (with a prefactor depending on the percentage of nodes fixed at time). In the next Section we explore the performance of the CI algorithm for different adaptive/decimation steps.

C. Effect of the percentage of fixed nodes during adaptive CI

In this section we show the performance of CI as a function of the percentage of removed nodes at each step of the adaptive algorithm. Indeed, removing a finite fraction of nodes at time reduces the time complexity from $N^2 \log N$ (corresponding to the one-by-one removal) to $N \log N$. In Extended Data Fig. 7 we show the effect of the percentage of fixed nodes at each adaptive step on an ER network of $N = 10^5$ nodes and average degree $\langle k \rangle = 3.5$. As the figure shows, the performance of CI is practically unaffected by the removal of up to 0.25% of nodes at time (i.e. 250 nodes for the considered network) compared to the one-by-one removal.

VI. COMPARISON WITH OTHER HEURISTIC METHODS

In the main text Fig. 2 we compare our solution with heuristics: high-degree and high-degree adaptive [9, 10], PageRank [7], kcore [12], eigenvector [33] and closeness [34] centralities. We also compare in Fig. 3, for Twitter and Mobile Networks, CI with HDA, HD, PR and k-core which are the only heuristics that are scalable to these large-scale datasets. It remains to compare our results with other popular heuristics which do not scale well with system size, and therefore we use smaller systems of 10^4 nodes: betweenness centrality [35] and equal-graph-partitioning [11]. We use the same size and parameters of the scale-free network used in [11]. The final comparison is with BP [14] and it will be done in the next section.

Betweenness centrality (BC) [35]. Betweenness centrality of node i is the sum of the fraction of all-pairs shortest paths that pass through i . BC is a very popular tool for network analysis, which has applications in different fields, from community detection to the human brain. However, it comes with a high computational cost that prevents the examination of large graphs of interest. The best algorithm for BC computations has $O(NM)$ time complexity for unweighted networks with N nodes and M vertices. It is not fast enough, for example, to handle our 10+ million people network. Extended Data Fig. 8 shows its performance. It does not outperform other centralities.

Equal-graph-partitioning (EGP) [11]. This method aims at dividing the network in clusters of equal size. It can behave well for homogeneous networks, like random regular graph, where an equal partition could be expected to destroy the network efficiently, but loses a lot of performance for heterogeneous networks, like scale-free networks, as we can see from Extended Data Fig. 8. Notice that we have used the same network parameters, size, and definition of EGP as given in [11] in the comparison of Extended Data Fig. 8. In fact, we reproduce the same curve and q_c as found for EGP in [11].

VII. COMPARISON WITH BELIEF PROPAGATION ALGORITHM OF ALTARELLI ET AL. [14]

The comparison with the Belief Propagation (BP) method proposed in Ref. [14] to optimally immunize a network deserves particular care, because this method does not apply

directly to the problem we are treating here. This is due to the fact that the parameter p in the work of Ref. [14] (which is noted as q in [14]) refers to the fraction of initially infected individuals. In our work the fraction p is assumed to be zero, because in epidemic outbreaks the number of initiators of the epidemic is very small, and typically of order $O(1)$ [46]. For instance, Sierra Leone’s explosion of Ebola cases in 2014 appeared to stem from one traditional healer’s funeral at which a single source infected 14 women; or the SARS outbreak in 2003 started when one doctor from China infected nine other guests in a Hong Kong hotel who then spread the virus throughout the city and to Vietnam and Canada (source- NY Times August 29, 2014, page A7, “Outbreak in Sierra Leone Is Tied to Single Funeral Where 14 Women Were Infected.”). Another example is the patient zero-hypothesis in the AIDS epidemics [47].

On the other hand the model of Ref. [14] is valid for $p > 0$, in particular, the results of Ref. [14] are illustrated for $p = 0.1$. The case $p = 0.1$ would imply an epidemic starting with 10% of the entire population infected independently at the same time. This would imply, for instance, 0.6 million people in Sierra Leone spontaneously and independently being infected at the same time, which would make any targeted immunization intervention perform equally well in practice. This result was shown by Ref. [14] in Fig. 12a: when $p > 0$ any reasonable targeted immunization method gives the same result for the fraction of infected nodes vs immunized nodes. [Fig. 12a in [14] treats the case of $p = 10\%$, noted as $q = 0.1$ in the notation of [14], and compares BP with greedy, HDA, eigenvector centrality and simulating annealing; all showing the same performance].

Therefore, the results of our paper are illustrated for $p = 0$. That being said, next, we compare our results with the BP algorithm in the closest possible regime to ours when $p \rightarrow 0$, and also for $p = 0.1$. In the limit $p \rightarrow 0$, BP becomes unfeasible because the time complexity of the BP algorithm diverges as p^{-3} for $p \rightarrow 0$, as we explain below. The results are shown in Extended Data Figs 9c and 10 and we observe that BP does not perform better than CI. Furthermore, the poor scalability of BP makes it prohibitive for the real networks of 10+ million people used in our work.

To perform a comparison, we need to briefly recall the approach of Ref. [14] and set the notation. The formulation of the problem is based on the long time limit of the SIR dynamics, which is described by the set of variables $\{\nu_i\}$, $i = 1, \dots, N$, giving the probability for each node to be infected after the epidemic outbreak (in Ref. [14] the variable ν_i is called

m_i , but we prefer to use ν_i to make contact with our notation). These variables satisfy the following equations:

$$\nu_i = p + (1 - p) \left[1 - \prod_{k \in \partial i} (1 - w\nu_{k \rightarrow i}) \right], \quad (107)$$

where the parameter p is the probability for node i to be initially infected; w is the probability that a given neighbor k of node i transmits the disease to i ; and the product on the r.h.s. is over all neighbours k of node i . The variable $\nu_{k \rightarrow i}$ (named $m_{k \rightarrow i}$ in Ref. [14]) is the probability that node k is infected in a modified network where node i is absent. Each $\nu_{i \rightarrow j}$ is associated with a directed edge $i \rightarrow j$ of the graph, and satisfies the following equation:

$$\nu_{i \rightarrow j} = p + (1 - p) \left[1 - \prod_{k \in \partial i \setminus j} (1 - w\nu_{k \rightarrow i}) \right]. \quad (108)$$

To include the effect of immunization, the authors of Ref. [14] introduce a binary variable σ_i for each node i , taking values $\sigma_i = +1$ if node i is immunized, and $\sigma_i = -1$ if not. Equations (107) and (108) then become:

$$\begin{aligned} \nu_i &= \frac{1 - \sigma_i}{2} \left\{ p + (1 - p) \left[1 - \prod_{k \in \partial i} (1 - w\nu_{k \rightarrow i}) \right] \right\} \equiv F_i(\sigma_i, \{\nu_{k \rightarrow i}\}_{k \in \partial i}), \\ \nu_{i \rightarrow j} &= \frac{1 - \sigma_i}{2} \left\{ p + (1 - p) \left[1 - \prod_{k \in \partial i \setminus j} (1 - w\nu_{k \rightarrow i}) \right] \right\} \equiv F_{i \rightarrow j}(\sigma_i, \{\nu_{k \rightarrow i}\}_{k \in \partial i \setminus j}). \end{aligned} \quad (109)$$

To find the optimal immunization set, Ref. [14] minimizes the following cost (energy) function $E(\sigma, \nu)$:

$$E(\sigma, \nu) = \sum_{i=1}^N \nu_i + \mu \sum_{i=1}^N \frac{1 + \sigma_i}{2} \equiv \sum_{i=1}^N e(\sigma_i, \nu_i), \quad (110)$$

where μ is a chemical potential controlling the fraction of immunized nodes. At this point, Ref. [14] applies the cavity method to estimate the single site marginal $P_i(\sigma_i)$, which gives the probability that node i is immunized. Approximating the network with a tree rooted on node i , the authors of Ref. [14] derive the following equation to assess the probability distribution $P_i(\sigma_i)$:

$$P_i(\sigma_i) \simeq \int \left(\prod_{k \in \partial i} d\nu_{k \rightarrow i} d\nu_{i \rightarrow k} Q_{k \rightarrow i}(\nu_{k \rightarrow i}, \nu_{i \rightarrow k}) \right) e^{-\beta e(\sigma_i, \nu_i)} \prod_{k \in \partial i} \delta[\nu_{i \rightarrow k} - F_{i \rightarrow k}], \quad (111)$$

where β is the inverse temperature, and the functions $Q_{k \rightarrow i}(\nu_{k \rightarrow i}, \nu_{i \rightarrow k})$ satisfy the following

BP equations:

$$Q_{i \rightarrow j}(\nu_{i \rightarrow j}, \nu_{j \rightarrow i}) \simeq \sum_{\sigma_i} \int \left(\prod_{k \in \partial i \setminus j} d\nu_{k \rightarrow i} d\nu_{i \rightarrow k} Q_{k \rightarrow i}(\nu_{k \rightarrow i}, \nu_{i \rightarrow k}) \right) e^{-\beta e(\sigma_i, \nu_i)} \prod_{k \in \partial i} \delta[\nu_{i \rightarrow k} - F_{i \rightarrow k}] . \quad (112)$$

Next, we iterate the BP equations to perform a comparison with our approach. These equations do not have an analytical solution, so that, following Ref. [14], we solve them numerically by discretizing the function $Q_{i \rightarrow j}(\nu_{i \rightarrow j}, \nu_{j \rightarrow i})$ in a number \mathcal{N}_{bin} of bins. The computational cost to update each message $Q_{i \rightarrow j}$ is of order $O(\mathcal{N}^{k_i-1})$, where k_i is the degree of node i . This makes the algorithm practically unfeasible on networks having nodes with large degree (think e.g. to scale free graphs). To overcome this problem, the authors of Ref. [14] use a convolution trick, which reduces the computational cost to $O((k_i - 1)\mathcal{N}_{bin}^3)$. Using the convolution method of Ref. [14], Eq. (112) reads:

$$Q_{i \rightarrow j}(\nu_{i \rightarrow j}, \nu_{j \rightarrow i}) \simeq e^{-\beta \mu} \left[\prod_{k \in \partial i \setminus j} \int d\nu_{k \rightarrow i} Q_{k \rightarrow i}(\nu_{k \rightarrow i}, 0) \right] \delta(\nu_{i \rightarrow j}) + \frac{1}{1-p} M^{(k_i-1)} \left(\frac{1-\nu_{i \rightarrow j}}{1-p}, (1-w\nu_{j \rightarrow i}) \frac{1-\nu_{i \rightarrow j}}{1-p} \right) e^{-\beta[1-(1-\nu_{i \rightarrow j})(1-w\nu_{j \rightarrow i})]} \Theta(\nu_{i \rightarrow j} - p) , \quad (113)$$

where the function $M^{(n)}(x, y)$ is defined iteratively by the convolution:

$$M^{(n)}(x, y) = \int_0^1 dx_1 dx_2 \delta(x - x_1 x_2) M^{(n-1)}(x_1, y) M^{(1)}(x_2, y) , \quad (114)$$

$$M^{(1)}(x, y) = \int_0^1 d\nu \delta[x - (1-w\nu)] Q \left(\nu, 1 - (1-p) \frac{y}{1-w\nu} \right) .$$

In all the following numerical results we will always use the efficient form (113) of the BP equations.

From the knowledge of the functions $Q_{i \rightarrow j}(\nu_{i \rightarrow j}, \nu_{j \rightarrow i})$, Ref. [14] computes the probability distribution $\mathcal{Q}_i(\nu_i)$ that node i has been infected during the epidemics [ν_i is defined in the first line of Eq. (109)], which is given by:

$$\mathcal{Q}_i(\nu_i) \simeq e^{-\beta \mu} \left[\prod_{k \in \partial i} \int d\nu_{k \rightarrow i} Q_{k \rightarrow i}(\nu_{k \rightarrow i}, 0) \right] \delta(\nu_i) + \frac{e^{-\beta \nu_i}}{1-p} M^{(k_i)} \left(\frac{1-\nu_i}{1-p}, \frac{1-\nu_i}{1-p} \right) \Theta(\nu_i - p) . \quad (115)$$

Moreover, they estimate the single spin marginal $P_i(\sigma_i)$ as:

$$P_i(\sigma_i) \simeq e^{-\beta \mu} \left[\prod_{k \in \partial i} \int d\nu_{k \rightarrow i} Q_{k \rightarrow i}(\nu_{k \rightarrow i}, 0) \right] \delta(\sigma-1) + \left[\int dx e^{-\beta[1-(1-p)x]} M^{(k_i)}(x, x) \right] \delta(\sigma+1) . \quad (116)$$

Once the authors of Ref. [14] obtained the probability distributions $\mathcal{Q}_i(\nu_i)$ and $P_i(\sigma_i)$, they can compute the average fraction of infected nodes f :

$$f = \frac{1}{N} \sum_{i=1}^N \int d\nu_i \nu_i \mathcal{Q}_i(\nu_i), \quad (117)$$

and the average fraction of immunized nodes q :

$$q = \frac{1}{N} \sum_{i=1}^N \frac{1 + \langle \sigma_i \rangle}{2} = \frac{1}{N} \sum_{i=1}^N \frac{1}{2} \left(1 + \sum_{\sigma_i} \sigma_i P_i(\sigma_i) \right). \quad (118)$$

A. BP adaptive

Before we compare BP with our method, we need to illustrate the BP method on a ER network to clarify some technical issues. We consider a small ER random graph of $N = 200$ nodes, where BP can be studied, and average degree $\langle k \rangle = 3.5$. We use the following values of the parameters: fraction of initially infected nodes $p = 0.1$, inverse temperature $\beta = 3.0$, and transmission probabilities $w = 0.4, 0.5, 0.6, 0.7$. The results are shown in Extended Data Fig. 9a, where we plot the fraction of infected nodes f versus the fraction of immunized nodes q . As already noticed in Ref. [14], we observe that, while for $w = 0.4$ the curve is continuous in the whole range of values of q , for larger values of w the curves get interrupted at a certain value of q . This is due to the fact (as mentioned by the authors of Ref. [14]) that the free-energy is non-convex in that region of values of q , and the chemical potential is flat as shown in Extended Data Fig. 9b. Therefore, all values of q in that region cannot be explored using the normal BP method. Physically, the fact that the thermodynamical potential becomes non-convex is the signature of a phase transition happening at a certain value of w . To overcome this problem, the authors of Ref. [14] suggest the following technique. One adds an extra magnetic field H to the energy function $E(\sigma, \nu)$ in Eq. (110), which is then adjusted at each update of the BP equations to keep fixed the value of immunized nodes q . We implemented this adaptive BP method (called 'fixed density BP' in Extended Data Fig. 9a), and we found that the missing part of the curve can be effectively reconstructed for some values of w larger than $w = 0.4$. Nonetheless, for even bigger values of w , we found that the missing part of the curve cannot be fully reconstructed, since the adaptive algorithm does not converge anymore. Usually the non-convergence of the BP algorithm is associated to the existence of a phase transition (different from the

aforementioned one), marking the limit of validity of the replica-symmetric cavity method. We then expect that for those values of q , where reconstruction is impossible, a different BP method has to be used, in order to deal with the phenomenon of replica symmetry breaking.

In the next Section we compare BP with CI in two different settings. The first case is the closest one to the regime where CI is defined (i.e. when $p \rightarrow 0$ and $w \rightarrow 1$). The second type of comparison is the case where $p > 0$ and the BP method can be used for all values of $q \in [0, 1]$.

B. Comparison

1. First comparison

Here, we compare BP in the closest possible regime to CI, i.e. for $p \rightarrow 0$ and $w \rightarrow 1$. Solving numerically the BP equations requires to discretize the functions $Q_{i \rightarrow j}(\nu_{i \rightarrow j}, \nu_{j \rightarrow i})$ in a number \mathcal{N}_{bin} of bins of the order $\mathcal{N}_{bin} \sim 1/p$, in order to have good numerical accuracy, because the smallest possible non-zero value assumed by ν_i is $\nu_i = p$, as stated in Ref. [14]. The BP running time is of order $O(M\mathcal{N}_{bin}^3)$, M being the number of edges in the graph. The factor \mathcal{N}_{bin}^3 comes from the computation of the function $M^{(n)}(x, y)$ in Eq. (114), that requires a double integration over x_1 and x_2 (giving a factor \mathcal{N}_{bin}^2), for each value of y (giving an extra factor \mathcal{N}_{bin}). Since $\mathcal{N}_{bin} \sim 1/p$, the BP running time diverges as p^{-3} for $p \rightarrow 0$. This is the reason why we cannot use BP directly for $p = 0$. So, we set $p = 0.01$, as small as possible, and $w = 0.99$, as close to 1 as possible, in the BP algorithm. Moreover, we choose a quite high value of the inverse temperature $\beta = 10$, close enough to the zero temperature limit. Note that for this value of $p = 10^{-2}$, the number of bins needed for good numerical resolution is of the order of $\mathcal{N}_{bin} \sim 10^2$, which introduces a prefactor in the computational cost of the algorithm already of order 10^6 .

We compare CI and BP on a small ER network of $N = 10^3$ nodes and average degree $\langle k \rangle = 3.5$, where BP can be run efficiently to do a study over the parameter space. Since for those values of p and w we cannot compute the full curve $f(q)$ (for the reasons explained in Section VII A), we compare the giant component found by BP and the one obtained with CI (notice that f coincides with the giant component G in the limits $p \rightarrow 0$ and $w \rightarrow 1$). In order to choose which nodes have to be removed according to BP, we use the following

criterion: we run BP and we assign to each node the value of the sign of its magnetization: $\text{sign}(\langle\sigma_i\rangle)$ (the value of the inverse temperature we chose, $\beta = 10$, is sufficiently high for the spins σ_i to be highly polarized). Then, node i is removed if $\text{sign}(\langle\sigma_i\rangle) = 1$, and it is not if $\text{sign}(\langle\sigma_i\rangle) = -1$. When BP does not converge, we stop the algorithm after a maximum number of iterations and we use the unconverged marginals to assign the magnetizations. In this way we can draw the full curve $G(q)$ even if BP does not converge. The result of the comparison is shown in Extended Data Fig. 9c, where we can see that BP is not better than CI, and performs slightly worse than the HDA method.

To conclude this section, we mention two other versions of the BP algorithm. The first one is developed in Ref. [48]. The technique used in Ref. [48] is the same BP technique as the one introduced by Altarelli *et al.* [13, 14]. From the analytical point of view, Ref. [48] improves the lower bound on the threshold q_c by considering the effects of 1 step replica symmetry breaking (1RSB), obtaining slightly larger lower bounds than those predicted by the replica symmetry (RS) approach of Altarelli *et al.*: $q_c^{\text{RS}} \leq q_c^{\text{1RSB}}$, or $\theta_{\min,0} \leq \theta_{\min,1}$, respectively in the notation of Ref. [48]. Hence the lower bound in Ref. [48] is larger than the one obtained by Altarelli *et al.*

The second variant of the BP algorithm is used in Refs. [49, 50] for solving the undirected feedback vertex set problem. This algorithm, named Belief Propagation Guided Decimation (BPD), improves the time complexity of the BP approach of [13, 14, 48] and can be tested in SF networks. In Extended Data Fig. 9d we compare the BPD with CI algorithm where we find evidence of the best performance of CI.

2. Second comparison

In this section we compare CI and BP in a different way; this time in the case where BP is well defined and CI is not, for parameter values $p \neq 0$ and $w \neq 1$. Thus, we use $p = 0.1$ and $w = 0.5$. So, this second comparison represents the opposite situation with respect to the previous one. We compare the two methods in the following way. We use BP to compute directly the fraction of infected nodes $f(q)$ as a function of the fraction q of immunized nodes by means of Eqs. (117)–(118). To compare against CI, we have to simulate explicitly the SIR process, since we cannot estimate directly the $f(q)$. More precisely, we first identify the immunized nodes with CI, and then we run the SIR algorithm to obtain the final fraction

of infected individuals $f(q)$.

The result of the comparison is reported in Extended Data Fig. 10, for an ER network of $N = 10^3$ nodes and average degree $\langle k \rangle = 3.5$. The values of the initially infected individuals p and the transmission probability w are $p = 0.1$ and $w = 0.5$. The value of the inverse temperature β used in the BP algorithm is $\beta = 10$ (for the portion of the curve where the adaptive BP algorithm is needed, we chose the lowest possible temperature such that the algorithm converges). As the figure shows, there is little difference between BP and CI, with CI slightly better for small q . Moreover we checked that even using HDA gives more or less the same results as BP and CI, as the authors of Ref. [14] also show in Fig. 12a of their work. Therefore, in the case when $p > 0$ (meaning that a finite fraction of the entire network is already infected from the very beginning of the epidemic outbreak), any reasonable targeted immunization technique gives the same result. That is, the optimization achieved by any method is washed out by the large number of already infected people, and all strategies perform equally well. On the contrary, in the case when $p = 0$, i.e. when the epidemic is initiated by a superspreader event $O(1)$, different strategies behave very differently, with CI being the best so far.

We notice, en passant, that the analytical BP estimation of $f(q)$ gives a lower bound on the actual $f(q)$. That is, if we used the same procedure as for CI, by first identifying the immunized nodes and then computing the fraction of infected ones through the outcome of the SIR process, the resulting curve $f(q)$ would lie above the analytical BP estimation.

Finally, we note that EO estimates the optimal numerical value of the threshold q_c as a numerical extrapolation to $N \rightarrow \infty$ and $\ell \rightarrow \infty$. While EO can estimate this threshold accurately (providing an upper bound very close to the real optimum), it cannot provide the actual optimal configuration \mathbf{n}^* for large system sizes. This is of course a general feature due to the NP-hardness of the problem.

Indeed, the EO method we use to estimate the value of optimal threshold for ER random graphs in Extended Data Fig. 4b may not be the only way to assess analytically that result. Indeed, there are other methods to approximate the location of the optimal threshold, which can provide lower or upper bounds. For instance, the BP (or cavity) method investigated above writes down approximate self-consistent equations for the optimization problem, that are solved iteratively to get an estimation of the optimal threshold. Often, the BP equations do not converge (as a consequence of the NP-hardness of the problem), but an attitude has

gained a foothold in the statistical physics community, which amounts to ignore convergence problems and use anyway an unconverged solution as an estimation of the optimal threshold. Indeed, in all cases where this approach has been pursued, it has been shown that the BP analytical prediction provides a lower bound to the optimal threshold. On the contrary, the EO method employed in our work provides an upper bound to the optimal threshold. Therefore, different analytical methods can give, indeed, predictions which are close to each other and, hence, close to the optimal value of the threshold.

Furthermore, it may not be impossible to find the exact analytical value of the threshold even if the problem is NP, as in the case of the Sherrington-Kirkpatrick model for spin glasses [36], where the Parisi ansatz provides the correct solution. We also notice that analytical solutions are based on the analysis of the most probable case in general, but not for a specific instance of the problem. Indeed, not every NP-complete problem can be analysed in this way. Some problems do not permit a discussion based on the most probable case. A random chosen satisfiability problem, for example, is almost always easy to solve, because a random sequence of symbols almost always does not make sense.

In our problem of optimal percolation, even though the numerical value of the threshold could be known exactly with EO or other method, the main problem remains open: finding an optimal configuration that is as close to the minimal as possible in the large system size. The most relevant challenge for practical applications of NP problems is not to estimate theoretically the value of the threshold q_c , but to find a scalable algorithm (for realistic applications should be at most $O(N \log N)$) which is able to approximate as close as possible a real optimal configuration \mathbf{n}^* at q_c .

Our algorithmic solution to this NP problem is then CI: a scalable algorithm $\sim O(N \log N)$ that contains the physics of the optimal configuration, and it is necessarily an approximation to the true optimum; being a $O(N \log N)$ algorithm it cannot give the optimal solution unless $P = NP$. Thus, proper benchmarking does not compare the analytical value of the threshold q_c . Benchmarking should be carried out by comparing the optimal configurations with the corresponding giant components for large size networks, which should be at least of the order of 10^7+ nodes (as we have done in Fig 3d), showing an improvement both in the running time and efficiency.

VIII. A NEW PARADIGM OF INFLUENCE IN SOCIAL MEDIA: TWITTER

In the next two sections we show that the performance of our method is confirmed in two real networks. We study two prototypical examples of real networks: Twitter web and a social network derived from phone calls. The former is used to test our theory as a new paradigm of influence, while the second can be used to design an immunization protocol in the case of an epidemic outbreak.

We have paved the way to explore the consequences of our theory in real networks, where the assumption of tree-like structure that is the basis of our theory is not necessarily satisfied. The reason to be interested in such a kind of problem is that it is manifestly in the interest of man's communal existence to understand how people increase their influence when they tie one another. The critical question is to what extent one can define a measure for influence solely on the basis of social contact network. The answer might be hard to find, but, at the same time, one cannot deny that the network itself mirrors the mutual relations of users, and hence it must contain information about their influence. The resulting network-based influence estimation can always be supplemented by measures of activity and engagement.

With this caveat in mind, our optimal percolation theory uncovers the optimal influencers in social media. In this context, the measure of node-influence in social media is the drop in the size of the giant cluster which would happen if the node in question were removed. Such a measure of influence is related to the ability to spread the news to the largest portion of the network as shown by our mapping of the maximal spreading problem in LTM (with $\theta_i = k_i - 1$) to optimal percolation. We test this idea in Twitter, next.

Twitter is the online social networking and microblogging service that has gained worldwide popularity. Here we use the dataset of approximately 16 million tweets sampled between January 23rd and February 8th, 2011 and publically shared by Twitter (<http://trec.nist.gov/data/tweets/>) (also available at <http://jamlab.org>, see Ref. [19] for more details). The natural way to get the social network is to extract the follower network through Twitter API. Unfortunately, due to the access rate limit of Twitter API, it is impossible to obtain the full information of the follower network in a reasonable time. Furthermore, many of the follower links are not active. To approximate the social network, we use an alternative way - the mention network [19]. In contrast to the normal tweets, mentions are tweets containing @username and usually include personal conversations or

references. In fact, the mention links have stronger strength of ties than follower links. Therefore, the mention network can be viewed as a stronger version of interactions between Twitter users. In the mention network, if user i mentions user j in his/her tweets, there exists a link from i to j . In order to better represent the social contacts, we also add to the network the retweet relations from the tweets. A retweet (RT @username) corresponds to content forward with the specified user as the nominal source. If user i retweets a tweet of user j , then a contact is established between j and i . We then consider all links to be undirected. In this way, the social network of Twitter is constructed. The resulting network has $N = 469,013$ nodes and $M = 913,457$ edges.

We measure the collective influence of a group of nodes as the drop in the size of the giant component which would happen if the nodes in question were removed. The results are shown in Fig. 3a, showing the better performance of CI in comparison with HDA, PR, HD and k-core. The other heuristics and BP cannot be run in this large dataset.

In Fig. 3b we plot the percentage of fake influencers (PFI) or false positives as a function of the fraction of removed nodes q . This quantity is defined with respect to the HD method, and represents the amount of different influencers between HD and CI. More precisely, we call $S_{\text{CI}}(q)$ the set of influencers (i.e. removed nodes) found by CI at a given value of q :

$$S_{\text{CI}}(q) = \{x_{\text{CI}}^1, x_{\text{CI}}^2, \dots, x_{\text{CI}}^{Nq}\}, \quad (119)$$

and $S_{\text{HD}}(q)$ the corresponding vector for HD. Moreover we denote by $|S(q)| = Nq$ the size of the set. Notice that $|S_{\text{CI}}(q)|$ is upper bounded by Nq_c^{CI} , i.e. $|S_{\text{CI}}(q)| \leq Nq_c^{\text{CI}}$, where q_c^{CI} is the influence threshold obtained with CI. Indeed Nq_c^{CI} is the maximum number of influencers. Analogously, $|S_{\text{HD}}(q)|$ is upper bounded by Nq_c^{HD} .

We define PFI(q) as:

$$\text{PFI}(q) = 100 \times \left[1 - \frac{|S_{\text{CI}}(q) \cap S_{\text{HD}}(q)|}{Nq} \right]. \quad (120)$$

In other words, we measure the percentage of different nodes removed by CI and HD. As shown in Fig. 3b, the PFI at the critical threshold of CI is $\text{PFI}(q_c^{\text{CI}}) \sim 26\%$, meaning that HD misses roughly 1/4 of the total number of (real, i.e. optimal) influencers. As a consequence the giant component for HD is still very large, $G_{\text{HD}}(q_c^{\text{CI}}) \sim 0.37$, and hence, HD needs to keep on removing nodes to fragment completely the network. This comes at the price of including a large number of fake influencers at the end of the process q_c^{HD} , where $\text{PFI}(q_c^{\text{HD}}) \sim 48\%$.

In the same way, if one knew the true (optimal) configuration of influencer, one could analogously define the fake CI influencers which do not overlap with the optimal ones. Actually, the obtained nearly optimal set by the CI method has an unknown overlap with the true optimal solution. On the other hand, the impossibility to find such an optimal set (because of the aforementioned prohibitive running time), makes the CI influencer set the natural substitute for the optimal one, and, hence, the reference set for studying the overlap with node sets identified by other methods.

IX. HALTING EPIDEMICS: MOBILE PHONE CALL NETWORK

While medicine has made solid advances in the isolation of new vaccines for an increasing number of diseases, and may expect to make still greater ones, no certain claim can be established for a corresponding advance in preventive immunization.

It is of deep social importance to have a fast and optimal intervention strategies when new outbreaks of disease break out. Prevention methods are still limited for various reasons: many virus are responsible of diseases of animals that can be transmitted to humans and thus causing epidemics. It is difficult, if not impossible, to control the populations of vectors and natural reservoirs, or predict what changes in the environment can favor the epidemics. The development of new drugs is usually not the solution to the problem.

It is generally accepted that an efficient way to fight epidemic diseases is the execution of immunization protocols and fast quarantine procedures, together with the spread of the knowledge of these dangers and the efforts to remove the environmental causes that favor them [46]. Probably a certain percentage of diseases will always remain undefeated, but if only one can succeed in reducing to a minority the majority that is today vulnerable, one will have accomplished a great deal, perhaps indeed everything that can be accomplished. In this situation is highly desirable to have a guiding strategy which enables to select who must be vaccinated or put in quarantine. Our theory offers a protocol of selection, the closest one to the optimal. This result is important because immunization doses can be limited or very expensive in practice, and without an optimal distribution these resources can go inadvertently to waste.

To investigate the applicability of CI to an immunization/quarantine scheme in a real large-scale social network we consider a social contact network built from the mobile phone

calls between people in Mexico. Data has been provided by GranData.

A mobile phone call social network reflects people's interactions in social lives, and is generally accepted as a proxy of a human contact network. For example, the mobile phone network from Mexico can help us to design effective immunization strategies, by identifying the most relevant social contacts among people. The disease spreads through direct contacts of infected people and proximity and mobility data from mobile phone networks can serve as a proxy of human movements and possible spreading patterns in human contact networks.

In order to build the network, we put a link between two people if there is a reciprocal exchange of phone calls between them in a observation window of three months (i.e. a call in both directions), and the number of such reciprocal calls is larger than or equal to three. This criterion gives us a network of $N = 14,346,653$ nodes, with an average degree $\langle k \rangle = 3.53$ and a maximum degree $k_{\max} = 419$. The result of the CI algorithm, compared to HD and HDA, is shown in Fig. 3d.

The phone call network is the prototype of big-data, where a scalable (i.e. almost linear) algorithm is mandatory. Indeed, the size of this network already rules out many heuristic methods with quadratic (or larger) running time (CC, EC, BC, and EGP) and also BP. From the perspective of performance, CI is better by a very good margin. Indeed, it fragments the network using about 500,000 people less than the best heuristic strategy (HDA) implying a saving of the same number of vaccines in a hypothetical immunization campaign. Moreover, when CI gives a zero giant component, HDA gives still $G \sim 0.3$, i.e. a connected network of $\sim 4 \times 10^6$ people. This result, together with the result on Twitter, indicates that, although the theory has been developed for a locally-tree like network, in real networks with loops the CI-algorithm performs quite well as well.

-
- [31] Colizza, C., Flammini, A., Serrano, M. A. & Vespignani, A. Detecting rich-club ordering in complex networks. *Nature Phys.* **2**, 110-115 (2006).
- [32] Wasserman, S. & Faust, K. *Social Network Analysis* (Cambridge Univ. Press, Cambridge, 1994).
- [33] Straffin, P. D. Linear algebra in geography: eigenvectors of networks. *Mathematics Magazine* **53**, 269-276 (1980).

- [34] Bavelas, A. Communication patterns in tasks oriented groups. *J. Acoust. Soc. Am.* **22**, 271-282 (1950).
- [35] Freeman, L. C. A set of measures of centrality based on betweenness. *Sociometry* **40**, 35-41 (1977).
- [36] Mézard, M. & Montanari, A. *Information, Physics, and Computation* (Oxford University Press, USA, 2009).
- [37] Centola, D., Eguiluz, V. & Macy, M. W. Cascade dynamics of complex propagation. *Physica A: Statistical Mechanics and its Applications* **374**, 449-456 (2007).
- [38] Singh, P., Sreenivasan, S., Szymanski, B. K. & Korniss, G. Threshold-limited spreading in social networks with multiple initiators. *Sci. Rep.* **3**, 2330 (2013).
- [39] Baxter, G. J., Dorogovtsev, S. N., Goltsev, A. V. & Mendes, J. F. F. Bootstrap percolation on complex networks. *Phys. Rev. E* **82**, 011103 (2010).
- [40] Wormald, N. C. The asymptotic connectivity of labelled regular graphs. *J. Combinatorial Theory B* **31**, 156-167 (1981).
- [41] Dorogovtsev, S. N., Mendes, J. F. F. & Samukhin, A. N. Metric structure of random networks. *Nucl. Phys. B* **653**, 307-338 (2003).
- [42] Bhatia, N. P. & Szegő, G. P. *Stability theory of dynamical systems* (Springer-Verlag, Berlin Heidelberg, 2002).
- [43] Šulc, P. & Zdeborová, L. Belief propagation for graph partitioning. *J. Phys. A: Math. Theor.* **43**, 285003 (2010).
- [44] Parisi, G., Ritort, F. & Slanina, F. Several results on the finite-size corrections in the Sherrington-Kirkpatrick spin-glass model. *J. Phys. A: Math. Gen.* **26**, 3775-3790 (1993).
- [45] Bray, A. J. & Moore, M. A. Chaotic nature of the spin-glass phase. *Phys. Rev. Lett.* **58**, 57-60 (1987).
- [46] Ferguson, N. M., *et al.* Strategies for containing an emerging influenza pandemic in Southeast Asia. *Nature* **437**, 209-214 (2005).
- [47] Auerbach, D. M., Darrow, W. W., Jaffe, H. W. & Curran, J. W. Cluster of cases of the acquired immune deficiency syndrome. Patients linked by sexual contact. *Am. J. Med.* **76**, 487-492. (1984).
- [48] Guggiola, A., Semerjian, G. Minimal contagious sets in random regular graphs. *J. Stat. Phys.* **158**, 300-358. (2015).

- [49] Zhou, H.-J. Spin glass approach to the feedback vertex set. *Eur. Phys. J. B* **86**, 455-463 (2013).
- [50] Qin, S.-M. & Zhou, H.-J. Solving the undirected feedback vertex set problem by local search. *Eur. Phys. J. B* **87**, 273 (2014).